Quasi-periodic oscillations, mass and jets of black holes: XTE J1550–564 and Sgr A*

Jacob Biemond*

Vrije Universiteit, Amsterdam, Section: Nuclear magnetic resonance, 1971-1975
**Postal address: Sansovinostraat 28, 5624 JX Eindhoven, The Netherlands*
Website: http://www.gewis.nl/~pieterb/gravi/ Email: gravi@gewis.nl

ABSTRACT

In this paper the recently proposed three tori model for the explanation of three high frequency quasi-periodic oscillations (QPOs) has been applied to black holes. The circular tori are: an outer torus with charge Q_o, a torus with mass m_m in the middle and an inner torus with charge Q_i, whereas the star bears a charge Q_s. Especially, the *gravitational* interaction between the torus with mass m_m and the masses of the other two tori has been taken into account in this work.

For the explanation of four low frequency QPOs a special interpretation of the gravitomagnetic theory has again been applied.

Predictions of the new model are compatible with deduced high and low frequency QPOs of the stellar black hole XTE J1550–564 and the supermassive black hole Sgr A*. Moreover, the Lense-Thirring precession frequency for black holes is discussed. Furthermore, it is shown, that a massive torus around Sgr A* may lead to a *higher* and *anisotropic* observed mass for the black hole. Finally, the origin of jets is investigated by studying the radial motion of charge in the Kerr-Newman space-time. It is shown that charge may be bound on a shell slightly outside the ergosphere.

1. INTRODUCTION

Quasi-periodic oscillations (QPOs) have been observed for many accreting pulsars, black holes and white dwarfs. Data from pulsars and black holes have been reviewed by, e.g., van der Klis [1]. In this work QPO frequencies of the stellar black hole XTE J1550–564 and the Galactic Center black hole Sgr A* will be considered more in detail. Recently, Miyoshi *et al.* [2] distinguished a series of seven QPOs for Sgr A*, obtained from radio emissions observed by the *Very Long Baseline Array* (*VLBA*). Previously, Aschenbach *et al.* [3, 4] distinguished more than seven QPOs from X-ray flares of Sgr A*, detected by *Chandra* in 2000 and by *XMM-Newton* in 2002.

QPOs are important from the theoretical point of view, for they may originate near the surface of the star, where effects predicted by general relativity may become manifest. Numerous models have been proposed to explain the origin of QPOs, but none is generally accepted. Orbital motions, including general relativistic epicyclic motions, and disk oscillations are the mechanisms most often considered for pulsars and black holes (see for a review, e.g., [1, § 2.8–§ 2.12]). Models involving orbital motions are usually given in terms of four basic formulas following from general relativity (see, e.g., [1]): a Kepler-like orbital frequency of neutral particles, ν_m, the so-called *radial* and *vertical* epicyclic frequencies, ν_r and ν_v, and the standard expression for the Lense-Thirring precession frequency, ν_{LT}.

As an example, for pulsars and black holes the so-called relativistic precession model was first proposed by Stella and Vietri (see, e.g., Stella, Vietri and Morsink [5]). In this model three formulas for the QPO frequencies were given. The QPO with the highest

frequency, the so-called *upper* kHz QPO, ν_u, was identified with a Kepler-like orbital frequency of neutral particles, ν_m, whereas the *lower* kHz QPO, ν_l, was attributed to the so-called periastron precession frequency, defined by $\nu_l \equiv \nu_m - \nu_v$. A third lower frequency QPO was identified with the Lense-Thirring precession frequency ν_{LT} of the Kepler-like orbital with frequency ν_m.

Motivated by the observation of the double peak kHz QPOs, the upper kHz QPO, ν_u, and the lower kHz QPO for many pulsars, ν_l, Kluźniak and Abramowicz [6, 7] tried to explain the two highest QPO frequencies of black holes in terms of the Kepler-like orbital frequency, ν_m, and the *radial* epicyclic frequency, ν_r. In addition, they proposed resonances between the frequencies ν_r and ν_m, e.g., $\nu_r : \nu_m = 3:1$. Moreover, they identified ν_u with ν_m and ν_l with the beat frequency $\nu_m - \nu_r$, resulting in the ratio $\nu_u/\nu_l = 3/2$. A related resonance model for XTE J1550–564 was given by Schnittman and Bertschinger [8]. Apart from resonances between the frequencies ν_r and ν_m, additional resonances may occur between ν_r and the *vertical* epicyclic frequency, ν_v. Several resonances between ν_r and ν_m or ν_v were discussed by Török [9], all resulting into a theoretical integer ratio $\nu_u/\nu_l = 3/2$. In addition, he gave a selection of observed values for ν_u and ν_l from four X-ray binary systems containing a black hole (including XTE J1550–564) and for the supermassive black hole Sgr A*, all yielding an approximate ratio $\nu_u/\nu_i = 3/2$.

Compared with other models, we have recently introduced charge as a possible new key ingredient [10]. The high frequency QPOs of white dwarfs, pulsars and black holes are attributed to three orbital frequencies of circular tori around the central star. The first frequency ν_i is attributed to an *inner* torus containing a total electric charge Q_i. The sign of the charge of Q_i is assumed to be opposite to the sign of the total charge Q_s of the *star* or black hole. The second frequency ν_o is attributed to an *outer* torus with total charge Q_o (Q_o and Q_s have the same sign). Further, a third torus, containing a total electrically neutral mass m_m (the subscript m stems from *middle*) is assumed to be present between the two other tori. The latter torus generates a third frequency, the Kepler-like frequency, ν_m. Furthermore, it is assumed that the high frequencies follow the sequence $\nu_i > \nu_m > \nu_o$. Thus, the frequency ν_m in our model is attributed to the second highest QPO frequency, whereas Stella, Vietri and Morsink [5] and Kluźniak and Abramowicz [6, 7] identify ν_m with the highest QPO frequency. It is noticed that usually elliptical orbits are considered in the relativistic precession model, whereas in our model only circular orbits are assumed.

By using Coulomb's law and classical mechanics, it has been shown, that an equilibrium between the charge Q_s of the star and the charges Q_o and Q_i in the tori may be possible. Equilibrium is only possible, if the angle between the planes of the tori is not too large. The motion of the tori becomes unstable, when the latter condition is not fulfilled. This instability may (partially) explain the observed instability of the quasi-periodic oscillations and the appearance of the high frequency QPOs ν_i and ν_o. The deduction of the latter frequencies is reviewed in section 2. In addition, expressions for the high frequency QPO, ν_m, from the third torus containing mass m_m, are also discussed in this section. Especially, the *gravitational* interaction between the torus with mass m_m and the masses of the other two tori has been taken into account in this work.

For the interpretation of the low frequency QPOs of pulsars and black holes another key ingredient may be essential, i.e., *a special interpretation of the gravitomagnetic theory*, which may be deduced from general relativity [10–14]. In this version the so-called "magnetic-type" gravitational field is identified as a common magnetic field. The resulting Lense-Thirring precession frequencies are deduced in ref. [10] and summarized in section 3. In addition, four new gravitomagnetic precession frequencies follow from this special interpretation (see ref. [10] and review in section 4 of this work). Furthermore, expressions for the parameter β^*, describing the strength of the magnetic field of stars, has been deduced in [10, 13] and reviewed in section 5. Data of XTE J1550–564 and Sgr A* are compared with the theoretical predictions in section 6.

It appears that the mass of the black hole Sgr A* is a crucial parameter in the interpretation of the observed QPOs. Ghez, Salim *et al.* [15, 16] reported masses of (3.7 ± 0.2)×$10^6 m_\odot$ and (4.1 ± 0.6)×$10^6 m_\odot$ for the central mass of the Galaxy, respectively. In addition, Schödel, Merrit and Eckart [17] deduced a best-fit black hole mass of (3.6 + 0.2/−0.4)×$10^6 m_\odot$. In our calculations a value of $m_s = 3.7\times10^6 m_\odot$ will be used. From the latter mass the following gravitational radius r_g can be calculated for Sgr A*

$$r_g \equiv \frac{Gm_s}{c^2} = 5.465\times10^{11}\,\mathrm{cm}, \tag{1.1}$$

where G is the gravitational constant and c is the velocity of light in vacuum.
The space-time associated with a charged, rotating black hole is described by the Kerr-Newman metric (see, e.g., Misner, Thorne and Wheeler [18]). In the t, r, ϑ and φ coordinates of Boyer and Lindquist the latter metric is given by

$$\begin{aligned} ds^2 = g_{ij}dx^i dx^j = &\left(1-\frac{2r_g r - Q_s'^2 r_g^{\,2}}{\rho^2}\right)c^2dt^2 - \frac{\rho^2}{\Delta}dr^2 - \rho^2 d\vartheta^2 \\ &-\left(r^2+a^2+\frac{2r_g r - Q_s'^2 r_g^{\,2}}{\rho^2}a^2\sin^2\vartheta\right)\sin^2\vartheta\, d\varphi^2 + 2\left(\frac{2r_g r - Q_s'^2 r_g^{\,2}}{\rho^2}a\sin^2\vartheta\right)c\,dt\,d\varphi, \end{aligned} \tag{1.2}$$

where r_g is defined in (1.1). The specific angular momentum of the black hole a is defined by $a \equiv S/(m_s c)$ and the dimensionless parameter Q_s' by $Q_s' \equiv (G^{½}m_s)^{-1}Q_s$, whereas ϑ is the angle between the directions of the angular momentum **S** and the position vector **r** pointing from the centre of the black hole to a field point F. In addition, the quantities ρ and Δ are defined by

$$\rho^2 \equiv r^2 + a^2\cos^2\vartheta \quad \text{and} \quad \Delta \equiv r^2 - 2r_g r + a^2 + Q_s'^2 r_g^{\,2}. \tag{1.3}$$

When $\Delta = 0$ in (1.2), a singularity occurs. The radius of the inner and outer event horizon, r_- and r_+, respectively, are then given by

$$r_- = r_g - \left(r_g^{\,2} - a^2 - Q_s'^2 r_g^{\,2}\right)^{½}, \quad r_+ = r_g + \left(r_g^{\,2} - a^2 - Q_s'^2 r_g^{\,2}\right)^{½}. \tag{1.4}$$

Another singularity occurs when the metric component $g_{tt} = 0$, resulting into

$$r_{in} = r_g - \left(r_g^{\,2} - a^2\cos^2\vartheta - Q_s'^2 r_g^{\,2}\right)^{½}, \quad r_{out} = r_g + \left(r_g^{\,2} - a^2\cos^2\vartheta - Q_s'^2 r_g^{\,2}\right)^{½}, \tag{1.5}$$

where r_{in} and r_{out} are the radii of the inner and outer horizon of the so-called ergosphere, respectively.

Furthermore, the stability condition for bound circular orbits derived by Dadhich and Kale [19] will be considered. For a prograde circular equatorial orbit in Kerr-Newman space-time it can be written as

$$\begin{aligned} F \equiv\; & r_g r\left(-6r_g r + r^2 + 9Q_s'^2 r_g^{\,2} - 3a^2\right) \\ & -4Q_s'^2 r_g^{\,2}\left(Q_s'^2 r_g^{\,2} - a^2\right) + 8a\left(r_g r - Q_s'^2 r_g^{\,2}\right)^{3/2} \geq 0. \end{aligned} \tag{1.6}$$

In Schwarschild space-time where both $a = 0$ and $Q_s' = 0$, stable orbits are obtained for $r = 0$ and the innermost circular orbit $r_{ISCO} = 6r_g$. In the so-called extreme limit of the Reissner-Nordstrøm space-time ($a = 0$ and $Q_s' = 1$) stable orbits are obtained for $r = r_g$ and $r_{ISCO} = 4r_g$. In the extreme limit of Kerr space-time ($a = r_g$ and $Q_s' = 0$) only one stable orbit is obtained for $r_{ISCO} = r_g$. When a value of r_{ISCO} is known in Kerr space-time the value of a follows from (1.6) for $F = 0$.

The adopted value of mass m_s of Sgr A* is discussed in section 7. Expressions for an effective mass m(eff), related to m_s, are deduced for two orientations of a massive torus with respect to the orbital plane of a star orbiting around Sgr A*. It is appears that the value of m(eff) may become *higher* than m_s and *anisotropic*, depending on the orientations of the tori. Finally, in order to investigate the origin of jets, the radial motion of a small charge, say a proton, is investigated in section 8. It is shown, that the proton may be at rest at a distance slightly larger than the radius r_{out} of (1.5). A discussion of the QPO results is given in section 9. Conclusions are drawn in section 10.

2. HIGH FREQUENCY QUASI-PERIODIC OSCILLATIONS

In this section a review is given of the high frequency QPOs, recently presented by Biemond [10]. The high frequency QPOs are attributed to orbital frequencies of circular tori around a central black hole. Three different high frequency QPOs will be distinguished: the first frequency ν_i is attributed to an *inner* torus with radius r_i, containing a total charge Q_i. The sign of the charge of Q_i is assumed to be opposite to the sign of the total charge Q_s of the *star* or black hole. The second frequency ν_o is attributed to an *outer* torus with radius r_o, containing a total charge Q_o (Q_o and Q_s have the same sign). Further, a third torus with radius r_m, containing a total electrically neutral mass m_m (the subscript m stems from *middle*), is assumed to be present between the two other tori. Thus, it is assumed that $r_i < r_m < r_o$.

2.1 High frequency QPO ν_i, due to the inner torus with charge Q_i

First, the calculation of the high frequency QPO ν_i will be reviewed. We consider a circular torus containing a total charge Q_o, lying in an x-y plane at distance r_o from the origin O, as shown in figure 1. A radius vector $\mathbf{r}_i$ from O to a point charge dQ_i at field point F is fixed by the spherical coordinates r_i, θ and $\varphi = 0$. The absolute value of the position vector $\mathbf{r}$ from F to a point charge dQ_o in the torus with charge Q_o is then given by

$$r = r_o(1 + x^2 - 2x\sin\theta\cos\varphi)^{1/2}, \tag{2.1}$$

where x is defined by $x \equiv r_i/r_o$.

Using Coulomb's law, the component of the Coulomb force $d\mathbf{F}_{io}$ in the direction of $\mathbf{r}_i$ between the point charge dQ_o and point charge dQ_i at field point F can then be calculated to be

$$d\mathbf{F}_{io} = \frac{dQ_o dQ_i}{r_o^2}\frac{x - \sin\theta\cos\varphi}{(1 + x^2 - 2x\sin\theta\cos\varphi)^{3/2}}\mathbf{i}_i, \tag{2.2}$$

where the unit vector $\mathbf{i}_i$ is given by $\mathbf{i}_i = \mathbf{r}_i/|\mathbf{r}_i|$. It is noted that an additional contribution to the Coulomb force, $d\mathbf{F}_{io}'$, perpendicular to $d\mathbf{F}_{io}$ and lying in the x-z plane, has been neglected (It can be shown, that $d\mathbf{F}_{io}' = 0$ for field points F lying on the z or x axis). The following relation applies, when the charge distribution in the torus with total charge Q_o is homogeneous

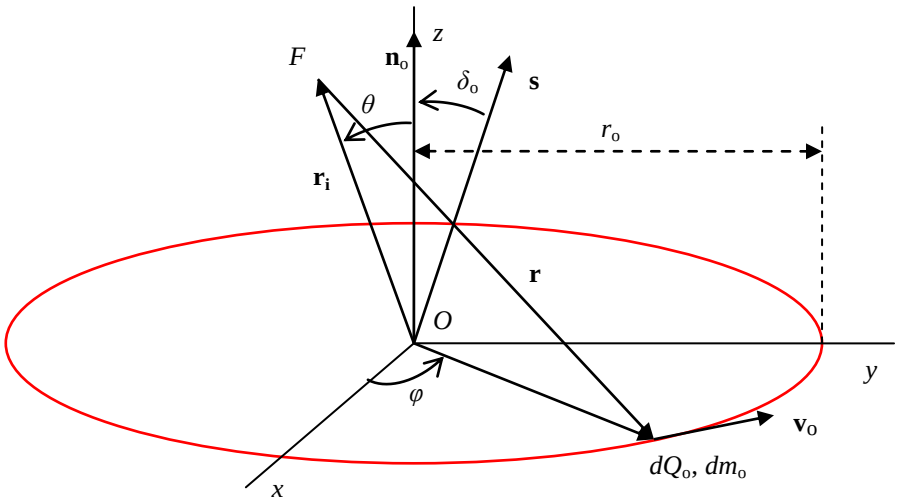

Figure 1. Spherical coordinates r_i, θ and $\varphi = 0$ of the field point F relative to the origin O and the spherical coordinates r_o, $\theta = 90^o$ and $\varphi = \varphi$ of point charge dQ_o (with point mass dm_o), lying in the x-y plane. The angle between the unit vector $\mathbf{s}$, defined as $\mathbf{s} \equiv \boldsymbol{\Omega}_s/\Omega_s$, and the unit vector $\mathbf{n}_o$ in the direction of the rotation axis of the torus with total charge Q_o is denoted by δ_o.

$$dQ_o = \frac{Q_o}{2\pi} d\varphi. \tag{2.3}$$

Substitution of the expression for dQ_o from (2.3) into (2.2), followed by integration of φ from 0 to π yields the following expression for the total Coulomb force $\mathbf{F}_{io}$ at field point F from the torus with total charge Q_o

$$\mathbf{F}_{io} = \frac{Q_o dQ_i}{\pi r_o^2} \int_0^\pi \frac{x - \sin\theta\cos\varphi}{(1 + x^2 - 2x\sin\theta\cos\varphi)^{3/2}} d\varphi\, \mathbf{i}_i = -f \frac{Q_o dQ_i}{r_o^2} \mathbf{i}_i. \tag{2.4}$$

Since the charge distribution in the circular torus is symmetric about $\varphi = 0$, the result of the integration for $\mathbf{F}_{io}$ yields no y component for $\varphi = 0$. The function f in (2.4) is defined by

$$f \equiv \frac{-1}{\pi x(1 + x^2 + 2x\sin\theta)^{1/2}} \left\{ K(k) - \frac{(1 - x^2)E(k)}{1 + x^2 - 2x\sin\theta} \right\}. \tag{2.5}$$

The integral of (2.4) can be calculated by using complete elliptic integrals of the first kind and second kind, $K(k)$ and $E(k)$, respectively. See for the properties of these integrals, e.g., [20, § 2.57, § 8.11–§ 8.12]. The modulus k of the elliptic integrals is given by

$$k^2 = \frac{4x\sin\theta}{1 + x^2 + 2x\sin\theta}. \tag{2.6}$$

We will treat some properties of this remarkable function f below.

If the star bears a point charge Q_s, a point charge dQ_i in the torus with total charge Q_i is subjected to the following Coulomb force $\mathbf{F}_{is}$

$$\mathbf{F}_{is} = \frac{Q_s dQ_i}{r_i^2} \mathbf{i}_i, \tag{2.7}$$

where $\mathbf{i}_i$ is again given by $\mathbf{i}_i = \mathbf{r}_i/|\mathbf{r}_i|$. It can be shown, however, that relation (2.7) remains

valid for the interaction between point charge dQ_i and a sphere with homogeneous charge density and total charge Q_s for any value of $r_i \geq r_s$. If equilibrium between the Coulomb forces $\mathbf{F}_{io}$ and $\mathbf{F}_{is}$ exists, combination of (2.4) and (2.7) yields the following relation

$$Q_s = x^2 f Q_o. \tag{2.8}$$

One can also say that the electric fields $\mathbf{F}_{io}/dQ_i$ due to Q_o (see (2.4)) and $\mathbf{F}_{is}/dQ_i$ due to Q_s (see (2.7)) compensate each other. Then, the resulting electric field at field point F is zero. Furthermore, it is noticed that equilibrium is only possible for a positive value of the function f. As an illustration, we calculate the value of f in some cases.

It appears that the value $\theta = 90^o$ is of particular interest. In that case, the modulus k from (2.6) reduces to $k^2 = 4x/(1+x)^2$ and the following simplified expression for f can be obtained from (2.5)

$$f = \frac{-1}{\pi x}\left\{\frac{K(k)}{1+x} - \frac{E(k)}{1-x}\right\} = \frac{-2}{\pi x}\left\{K(x) - \frac{E(x)}{1-x^2}\right\} \equiv f(x). \tag{2.9}$$

In deriving the right hand side of (2.9), use has been made of the following properties of the complete elliptic integrals: $K(k) = (1 + x)K(x)$ and $E(k) = \{2E(x)/(1 + x)\} - (1 - x)K(x)$ (see, e.g., [20, § 8.12]).

A second case follows from (2.5), when $f \equiv f_0 = 0$

$$K(k_0) = \frac{(1-x_0^2)E(k_0)}{1+x_0^2-2x_0\sin\theta_0}. \tag{2.10}$$

An additional relation between k_0, x_0 and θ_0 is given by (2.6). When a value for k_0 is chosen $K(k_0)$ and $E(k_0)$ can be found. Combination of (2.6) and (2.10) then yields the values for x_0 and θ_0. Further, it is noticed that k_0 and k can be written as

$$k_0 = \sin\alpha_0 \text{ and } k = \sin\alpha, \tag{2.11}$$

where α_0 and α are the so-called modular angles.

In table 1 a number of parameters occurring in (2.5), (2.6), (2.9), (2.10) and (2.11) are given (see more results in ref. [10] for additional high values of α_0). In order to calculate the various parameters the following procedure has been followed. First, a value of α_0 is chosen and k_0 is calculated from (2.11a). When k_0 is known, $K(k_0)$ and $E(k_0)$ are calculated from their respective series expansions up to sixth order terms (see, e.g., [20, § 8.11]). Then, x_0 and θ_0 can be calculated from (2.6) and (2.10). Subsequently, choosing $\theta = 90^o$ and $x = x_0$, the values of k and α can be calculated from (2.6) and (2.11b), respectively. When k is known, the complete elliptic integrals $K(k)$ and $E(k)$ are also calculated from their respective series expansions up to sixth order terms (see, e.g., [20, § 8.11]). For values of α_0 between, say $\alpha_0 = 30^o$ and $\alpha_0 = 55^o$, terms higher than sixth order become important. Therefore, less significant digits have been given for the calculated parameters in this range. It can be shown that the value of $\sin\theta_0$ approaches to $(⅔)^{½}$ (or $\theta_0 \rightarrow 54.74^o$) for small values of α_0. Finally, the value for f can be calculated from (2.9). It is noticed that for $x = x_0$ the charge system is only stable, if θ is lying in the interval $\theta_0 < \theta \leq 90^o$, corresponding to the interval $f_0 < f \leq f(x)$ for f.

A third case follows from (2.6), when $\theta = 0^o$. A value $k = 0$ is then obtained. Introduction of the quantities $\theta = 0^o$ and $k = 0$ into (2.5) yields for f

$$f = -\frac{x}{(1+x^2)^{3/2}}. \tag{2.12}$$

Note that f is negative for a positive value of x, so that no equilibrium can exist for this charge configuration. Summing up, the factor f is an important parameter with respect to the stability of the system.

In order to illustrate the property of sign change of function f, the following example will be considered. The plane of the torus with total charge Q_i and the plane of the torus with total charge Q_o are supposed to have the y axis in common. The charge elements dQ_i at the field point F in the x-z plane with the spherical coordinates r_i, $\theta = \theta$ and $\varphi = 0$ (see figure 2) and at the point with coordinates r_i, $\theta = 180^o - \theta$ and $\varphi = 180^o$ are less firmly bound (or in a non-bound state when $\theta < \theta_0$). However, the charges dQ_i at the coordinates r_i, $\theta = 90^o$ and $\varphi = 90^o$ and r_i, $\theta = 90^o$ and $\varphi = 270^o$ are in a bound state. As a result, the current flows in the tori may be interrupted twice per revolution around the star, so that their frequencies may become manifest. From the results in table 1 follows that values for θ_0 are only a little bit smaller than 90^o when x approaches to unity. The stability range for θ is thus rather limited for large values of x. In order to obtain a stable situation between the tori with charges Q_i and Q_o, respectively, the angle $\Delta = 90^o - \theta$ between the unit vectors $\mathbf{n}_i$ and $\mathbf{n}_o$ (see figure 2) has to be small. The sign change of the function f might thus explain the manifestation of the high frequency QPOs ν_i and ν_o. The occurrence of the high frequency QPO ν_m, however, is not explained by this mechanism. For simplicity reasons, it will be assumed in this work that the observed orbital frequencies ν_i, ν_o and ν_m represent the number of complete revolutions per second around the star with charge Q_s.

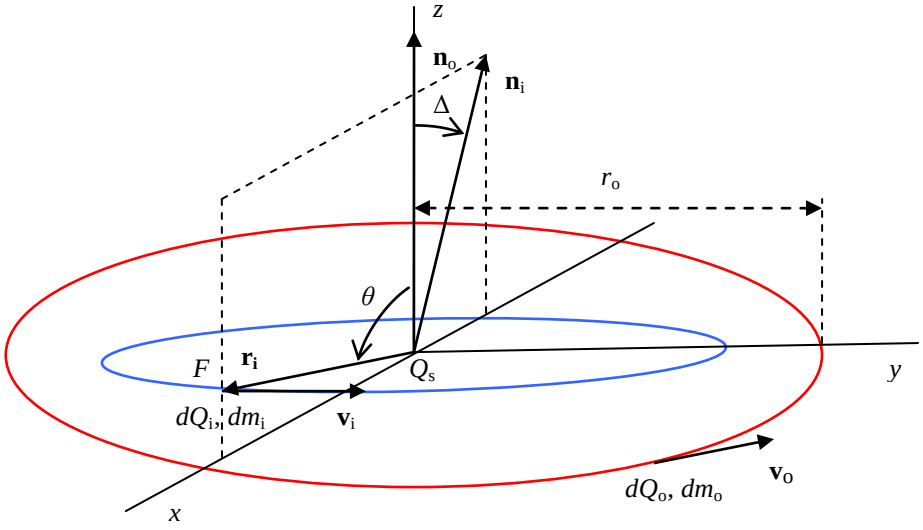

Figure 2. Orbits of the tori with total charge Q_o (red) and Q_i (blue), respectively. The direction of the positive z axis of the coordinate system is chosen along the rotation axis of the torus with charge Q_o. The unit vector in this direction is denoted by $\mathbf{n}_o$. The direction of the rotation axis of the torus with charge Q_i with unit vector $\mathbf{n}_i$ is chosen in the x-z plane. The angle between $\mathbf{n}_o$ and $\mathbf{n}_i$ is given by Δ. The field point F with spherical coordinates r_i, θ and $\varphi = 0$ is shown (see also text).

For the case considered in figure 2, the value of f can be calculated at the field point F of any point charge dQ_i. For example, for $\theta = \theta_0$ at the field points F (r_i, θ_0, $\varphi = 0$) and F (r_i, θ_0, $\varphi = 180^o$) $f = f_0 = 0$ and for both field points $F(r_i, \theta = 90^o, \varphi = 90^o)$ and $F(r_i, \theta = 90^o, \varphi = 270^o)$ $f = f(x)$ from (2.9). Likewise, other values for f can be calculated from (2.5). Subsequently, the average value of f over the whole orbit with total charge Q_i could be calculated. In our calculations, however, we will approximate the average value of f over the whole orbit, $\overline{f(x)}$, by $\overline{f(x)} = ½\{f_0 + f(x)\} = ½\{0 + f(x)\} = ½ f(x)$.

Table 1. Calculated values for k_0, x_0, θ_0, g_0 and f_0 ($f_0 = 0$), together with the values for $K(k_0)$ and $E(k_0)$ on the upper line. Choosing $\theta = 90^o$ and $x = x_0$, one obtains the values for k, $K(k)$, $E(k)$, $f(x)$ and $g(x)$. These values have been given on the lower line.

α_0 α	k_0 k	$K(k_0)$ $K(k)$	$E(k_0)$ $E(k)$	x_0 $x = x_0$	θ_0 (^{o}) θ (^{o})	f_0 $f(x)$	g_0 $g(x)$
89.50000	0.9999619	6.1278	1.0002	0.99907	89.001	0	1.952
89.97325	0.9999999	9.0565	1.0000	0.99907	90	340.2	342.8
89.00000	0.9998476	5.4349	1.0008	0.99670	88.01	0	1.733
89.90526	0.9999986	7.7911	1.0000	0.99670	90	95.48	97.65
88.0000	0.999391	4.7427	1.0026	0.98856	86.06	0	1.519
89.6703	0.999983	6.5441	1.0001	0.98856	90	27.08	28.87
85.0000	0.996195	3.8317	1.0127	0.94449	80.58	0	1.259
88.3640	0.999592	4.9432	1.0018	0.94449	90	5.225	6.554
80.0000	0.984808	3.1534	1.0401	0.83578	73.07	0	1.105
84.8679	0.995991	3.8060	1.0132	0.83578	90	1.560	2.624
75.0000	0.965926	2.7681	1.0764	0.71543	67.51	0	1.0468
80.4510	0.986144	3.1980	1.0372	0.71543	90	0.7922	1.754
70.0000	0.939693	2.5046	1.1184	0.60118	63.52	0	1.0212
75.5768	0.968483	2.8047	1.0719	0.60118	90	0.4956	1.413
65.000	0.90631	2.3088	1.1638	0.49903	60.71	0	1.0096
70.476	0.94250	2.5262	1.1142	0.49903	90	0.3437	1.2444
60.000	0.86603	2.1565	1.2111	0.40992	58.74	0	1.0043
65.259	0.90821	2.3177	1.1614	0.40992	90	0.2519	1.1498
55.000	0.8192	2.035	1.259	0.3330	57.37	0	1.0018
59.975	0.8658	2.156	1.211	0.3330	90	0.1900	1.0928
30.000	0.5000	1.686	1.468	0.0880	54.88	0	1.0000
33.047	0.5453	1.712	1.447	0.0880	90	0.0447	1.0058
20.0000	0.342020	1.6200	1.5238	0.038082	54.77	0	1.0000
22.0846	0.375975	1.6312	1.5137	0.038082	90	0.01908	1.0011
15.0000	0.25882	1.5981	1.5442	0.021228	54.75	0	1.0000
16.5792	0.28534	1.6043	1.5383	0.021228	90	0.01062	1.0003
10.0000	0.17365	1.5828	1.5589	0.009375	54.74	0	1.0000
11.0605	0.19185	1.5856	1.5562	0.009375	90	0.004688	1.0001
5.0000	0.08716	1.5738	1.5678	0.002335	54.74	0	1.0000
5.5326	0.09641	1.5745	1.5671	0.002335	90	0.001167	1.0000
3.0000	0.05234	1.5719	1.5697	0.000840	54.74	0	1.0000
3.3199	0.05791	1.5721	1.5695	0.000840	90	0.000420	1.0000
2.0000	0.03490	1.5713	1.5703	0.000373	54.74	0	1.0000
2.2133	0.03862	1.5714	1.5702	0.000373	90	0.000187	1.0000

In deriving (2.8), only Coulomb forces have been taken into account. When the gravitation law of Newton and the centrifugal force are also included, a more general description is obtained. When all these forces between a point mass dm_i with charge dQ_i in the inner torus, charge Q_s in the star and a charge Q_o in the outer torus are in equilibrium, the following relation applies

$$\frac{dm_i v_i^2}{r_i} = \frac{dm_i G m_s}{r_i^2} - \frac{dQ_i Q_s}{r_i^2} + f\frac{dQ_i Q_o}{r_o^2}, \tag{2.13}$$

where v_i is the velocity of dm_i moving in a circular orbit with radius r_i around the star with mass m_s. The charge Q_o and mass m_o both move in a circular orbit with radius r_o around the star ($r_i < r_o$). It is noticed that the gravitational attraction between the masses m_i and m_o in the tori and Lorentz forces in the considered system have been neglected. Moreover, no general relativistic effects have been taken into account in the derivation of (2.13). Starting from a Kerr-Newman space-time, Aliev and Galtsov [21] considered the

latter effects for the binary system of a charged star and a charged mass moving in a circular orbit around that star. As a result, equation (2.13) can only be considered as a first order approximation.

For a homogeneous mass and charge distribution in the torus with a total mass m_i and a total charge Q_i, respectively, the following relation applies

$$\frac{dQ_i}{dm_i} = \frac{Q_i}{m_i}. \tag{2.14}$$

Then, from (2.13) and (2.14) the following expression for the high frequency ν_i for a point mass dm_i with charge dQ_i in the torus with a total charge Q_i can be calculated

$$\nu_i = \frac{1}{2\pi}\left[\frac{Gm_s}{r_i^3}\left\{1 - \frac{m_s}{m_i}Q_i'\left(Q_s' - x^2 f Q_o'\right)\right\}\right]^{1/2}, \tag{2.15}$$

where Q_i' is defined by the dimensionless quantity $Q_i' \equiv (G^{1/2}m_s)^{-1}Q_i$, Q_s' by $Q_s' \equiv (G^{1/2}m_s)^{-1}Q_s$ and so on. It is to be expected that the factor m_s/m_i on the right hand side of (2.15) is large. In this work it will be assumed that the difference $(Q_s - x^2 f Q_o)$ is small, so that relation (2.8) remains approximately valid. The charge dependent contribution on the right hand side of (2.15) may then be positive or negative. As a result, the orbital frequency ν_i may thus be larger or smaller than the corresponding Kepler frequency $(2\pi)^{-1}(Gm_s/r_i^3)^{1/2}$.

2.2 High frequency QPO ν_o, due to the outer torus with charge Q_o

The high frequency QPO ν_i of (2.15) has been calculated for an inner torus with charge Q_i and radius r_i. Analogously, a high frequency QPO ν_o can be deduced, due to an outer torus with charge Q_o and radius r_o ($r_o > r_i$). We now consider a circular torus containing a total charge Q_i, lying in another x-y plane at distance r_i from the origin O (compare with figure 1). A radius vector $\mathbf{r}_o$ from O to field point F is fixed by the spherical coordinates r_o, θ and $\varphi = 0$. The absolute value of the position vector $\mathbf{r}$ from F to a point charge dQ_i in the torus with charge Q_i is then also given by (2.1).

Using Coulomb's law, Newton's gravitation law and the centrifugal force, the following expression for the frequency ν_o for a point mass dm_o with point charge dQ_o in the torus can be calculated (see for a detailed calculation ref. [10])

$$\nu_o = \frac{1}{2\pi}\left[\frac{Gm_s}{r_o^3}\left\{1 - \frac{m_s}{m_o}Q_o'\left(Q_s' + g Q_i'\right)\right\}\right]^{1/2}, \tag{2.16}$$

where m_o and Q_o are the total mass and the total charge in the outer torus of radius r_o, respectively. The dimensionless quantity Q_o' is defined by $Q_o' \equiv (G^{1/2}m_s)^{-1}Q_o$ and so on. It is to be expected that the factor m_s/m_o on the right hand side of (2.16) is large. In this work it will be assumed that the sum $(Q_s + g Q_i)$ is small, so that

$$Q_s \approx -g Q_i. \tag{2.17}$$

In principle, the charge dependent contribution on the right hand side of (2.16) may thus be positive or negative. The orbital frequency ν_o may thus be larger or smaller than the corresponding Kepler frequency $(2\pi)^{-1}(Gm_s/r_o^3)^{1/2}$.

The function g in (2.16) is defined by

$$g \equiv \frac{1}{\pi(1+x^2+2x\sin\theta)^{1/2}}\left\{K(k)+\frac{(1-x^2)E(k)}{1+x^2-2x\sin\theta}\right\}. \tag{2.18}$$

The quantity g of (2.18) can also be calculated by using the complete elliptic integrals of the first kind and second kind, $K(k)$ and $E(k)$, respectively. See for the properties of these integrals, e.g., [20, § 2.57, § 8.11–§ 8.12]. The modulus k of the elliptic integrals is again given by (2.6).

The general expression g of (2.18) will now be evaluated in two cases. For $\theta = 90^{\circ}$, the modulus k of (2.6) again reduces to $k^2 = 4x/(1+x)^2$, whereas g of (2.18) reduces to

$$g = \frac{1}{\pi}\left\{\frac{K(k)}{1+x}+\frac{E(k)}{1-x}\right\} = \frac{2}{\pi}\left\{\frac{E(x)}{1-x^2}\right\} \equiv g(x). \tag{2.19}$$

In deriving (2.19), use has again been made of the relations: $K(k) = (1+x)K(x)$ and $E(k) = \{2E(x)/(1+x)\} - (1-x)K(x)$ (see, e.g., [20, § 8.12]). Taking $x = x_0$, θ_0, k_0 from table 1, g_0 can be calculated from (2.18). Likewise, $g(x)$ can be obtained by inserting $x = x_0$ and k from table 1 into (2.19). Results for g_0 and $g(x)$ have been added to table 1 for a number of cases. It is noticed that values for g are always positive, whereas the value of f from (2.5) may become negative (see, e.g., (2.12)).

Analogously to the method followed for $\overline{f(x)}$, from (2.18) an average value for g can be calculated. For the case considered in figure 2, the value of g could be calculated at the field point F of any point charge dQ_o. Subsequently, the average value of g over the whole orbit with total charge Q_o could be deduced. Utilizing (2.19), in our calculations we will approximate $\overline{g(x)}$ by $\overline{g(x)} = \frac{1}{2}\{g_0 + g(x)\}$.

Using (2.8) and (2.17), it is possible to calculate the total charge Q_{tot} of the system. One obtains

$$Q_{tot} = Q_s + Q_i + Q_o = \left(1-\frac{1}{g}+\frac{1}{x^2 f}\right)Q_s. \tag{2.20}$$

This relation may be helpful to understand the loading mechanism of a star. Suppose, for example, that the quantity x will increase as a result of compression of the outer torus, due to accretion. Then, it follows from (2.20) and data in table 1, that the quantity $\{1 - 1/g + 1/(x^2 f)\}$ becomes less positive. Assuming that Q_{tot} is constant and that the charge Q_s is positive, the amount of positive charge Q_s will increase and positive charge must flow to the star. As an additional consequence, the Lorentz force will generate a toroidal current in the star, when the positive charge enters the star at the equator.

2.3 High frequency QPO ν_m, due to the middle torus with mass m_m

Finally, the orbital frequency ν_m for a point mass dm_m in a circular torus containing a homogeneous electrically neutral mass distribution with total mass m_m can be shown to be (compare with, e.g., Aliev and Galtsov [21])

$$\nu_m = \frac{1}{2\pi}\left(\frac{Gm_s}{r_m^3}\right)^{1/2}\frac{1}{1+\dfrac{S}{c^2 m_s}\left(\dfrac{Gm_s}{r_m^3}\right)^{1/2}} = \frac{1}{2\pi}\left(\frac{Gm_s}{r_m^3}\right)^{1/2} f_s, \tag{2.21}$$

where r_m is the radius of the torus with mass m_m. It is noticed that equation (2.21) applies to prograde motion of dm_m in the equatorial plane around the star. This Kepler-like frequency ν_m was used by many authors (see, e.g., [4, 5, 8–10]). For white dwarfs and

pulsars the relativistic factor f_S in (2.21) depending on the angular momentum S usually approaches unity, so that the radius r_m can be approximated by the Kepler radius r_K

$$r_K = \left\{ \frac{Gm_s}{(2\pi\nu_m)^2} \right\}^{1/3}. \tag{2.22}$$

However, the latter approximation is probably not valid for the supermassive black hole Sgr A*.

Furthermore, the contributions from the gravitational interactions between the mass m_m in the torus with radius r_m in the middle and masses m_i and m_o in the tori with radii r_i and r_o, respectively, can be accounted for. Application of the same method followed in the deduction of (2.15) and (2.16), yields the following expression for the frequency ν_m

$$\nu_m = \frac{1}{2\pi} \left\{ \frac{Gm_s}{r_m^3} \left(1 + g(x_i)\frac{m_i}{m_s} - x_o^2 f(x_o)\frac{m_o}{m_s} \right) \right\}^{1/2}, \tag{2.23}$$

where x_i and x_o are defined by $x_i \equiv r_i/r_m$ and $x_o \equiv r_m/r_o$. It is stressed that equation (2.23) applies to the case where all tori with mass m_i, m_m and m_o are lying in the same plane. The quantities $f(x_o)$ and $g(x_i)$ in (2.23) can be found from (2.9) and (2.19), respectively

$$f(x_o) = \frac{-2}{\pi x_o} \left\{ K(x_o) - \frac{E(x_o)}{1-x_o^2} \right\}, \quad g(x_i) \equiv \frac{2}{\pi} \left\{ \frac{E(x_i)}{(1-x_i^2)} \right\}. \tag{2.24}$$

It is noticed that the velocities v_i in (2.13), and the corresponding velocities v_m of dm_m and v_o of dm_o moving in a respective circular orbit of radius r_m and r_o around the star are usually non-relativistic for white dwarfs and pulsars. For a supermassive black hole the velocities v_i, v_m and v_o may become relativistic, however, so that other terms may also contribute to the expression of ν_m of (2.23). It is noticed that the frequencies ν_i from (2.15), ν_o from (2.16) and ν_m from (2.23) have all been obtained by application of simple classical mechanics and Coulomb's law. Furthermore, none of these orbital frequencies depend on the rotational frequency ν_s of the star. In section 5 of this work it will be shown how the influence of ν_s may become manifest in another way.

In section 3 we will now discuss the interpretation of the gravitomagnetic field and the Lense-Thirring precession.

3. GRAVITOMAGNETIC FIELD AND LENSE-THIRRING PRECESSION

For the explanation of the low frequency QPOs of pulsars and black holes a special interpretation of the gravitomagnetic theory will be used. In this version, which may be deduced from general relativity [10–14], the so-called "magnetic-type" gravitational field is identified as a common magnetic field. Following this approach, the Lense-Thirring precession frequency and four new gravitomagnetic precession frequencies have recently been deduced [10]. The latter precession frequencies will shortly be discussed in section 4.

First, it is noticed, that our interpretation of the gravitomagnetic field leads to a prediction of the strength of the magnetic field of stars and black holes. Identification of the "magnetic-type" gravitational field with a magnetic field results into the so-called Wilson-Blackett formula. This relation applies, e.g., to a spherical star consisting of electrically neutral matter

$$\mathbf{M}(\mathrm{gm}) = -\tfrac{1}{2}\beta c^{-1} G^{1/2} \mathbf{S}. \tag{3.1}$$

Here **M**(gm) is the gravitomagnetic dipole moment of the star with angular momentum **S**, and β is a dimensionless constant of order unity. Available observations and theoretical considerations with respect to the relation (3.1), and other explanations of the origin of the magnetic field of celestial bodies have been reviewed by Biemond [12]. The magnetic fields of pulsars have separately been discussed [13]. The angular momentum **S** for a spherical star with mass m_s and radius r_s can be calculated from the relations

$$\mathbf{S} = I\boldsymbol{\Omega}_s, \text{or } S = I\,\Omega_s = \tfrac{2}{5}\, f_s m_s r_s^2 \Omega_s, \tag{3.2}$$

where $\Omega_s = 2\pi\nu_s$ is the angular velocity of the star (ν_s is its rotational frequency), I is the moment of inertia of the star and f_s is a dimensionless factor depending on the homogeneity of the mass density in the star (for a homogeneous mass density $f_s = 1$). For convenience sake, a value $f_s = 1$ will be assumed in this work.

Since no stellar radius r_s occurs in the Kerr or Kerr-Newman metric, equation (3.2) cannot be used for the calculation of the angular momentum S. The latter quantity, however, can be written as (see, e.g., Misner, Thorne and Wheeler [18])

$$S = cm_s a, \tag{3.3}$$

where a is the specific angular momentum. Note that the non-relativistic expression for the angular momentum S of (3.2) contains the stellar radius r_s, whereas S in (3.3) depends on distance a. A special limiting case occurs, when a is taken equal to r_g. For Sgr A* combination of (1.1) and (3.3) then yields for S

$$\frac{a}{r_g} = 1 \rightarrow S = \frac{Gm_s^2}{c} = 1.206\times10^{62}\,\text{g.cm}^2.\text{s}^{-1}. \tag{3.4}$$

It is noticed that for the choices $a = r_g$ and $Q_s = 0$, i.e., in the extreme Kerr space-time, both event horizons r_- and r_+ from (1.4) reduce to r_g, whereas for $a = r_g$, $\vartheta = 90^o$ and $Q_s = 0$ r_{out} from (1.5) reduces to $2r_g$.

The value of a gravitomagnetic dipole moment **M** (or an electromagnetic dipole moment **M**) can be calculated from

$$\mathbf{M} = \tfrac{1}{2} R^3 \mathbf{B}_p, \text{ or } M = \tfrac{1}{2} R^3 B_p. \tag{3.5}$$

Here $\mathbf{B}_p$ is the magnetic induction field at, say, the north pole of the star at distance R from the centre of the star to the field point where $\mathbf{B}_p$ may be observed ($R \geq r_s$).

Combination of (3.1), (3.2) and (3.5) yields the following gravitomagnetic prediction for $\mathbf{B}_p$

$$\mathbf{B}_p(\text{gm}) = -\tfrac{2}{5}\beta c^{-1} G^{\frac{1}{2}} m_s r_s^{-1} \boldsymbol{\Omega}_s. \tag{3.6}$$

The minus sign reflects that the vectors $\mathbf{B}_p$(gm) and $\boldsymbol{\Omega}_s$ possess opposite directions for $\beta = +1$. Neither the sign nor the value of β follows from the gravitomagnetic theory. It is stressed that $\mathbf{B}_p$(gm) at distance r_s has been derived for an ideal gravitomagnetic dipole located at the centre of the star. For a homogeneous mass distribution in the star, however, the same result for $\mathbf{B}_p$(gm) can be deduced [22]. For $a = r_g$ and $Q_s' = 0$ combination of (3.1), (3.3) and (3.5) yields the following expression for B_p(gm) at distance $R = r_g$ from the centre of Sgr A*

$$B_{\rm p}({\rm gm}) = -\beta G^{1/2} m_{\rm s} r_{\rm g}^{-2} = -6.4\times10^{12}\,\beta \text{ Gauss.} \tag{3.7}$$

Note that for lower values of the angular momentum S the absolute value of $B_{\rm p}$(gm) becomes smaller. In sections 5 and 6.3 the result of (3.7) will further be discussed.

In addition, precession phenomena are another consequence of the gravitomagnetic theory. The theory predicts an angular precession velocity $\mathbf{\Omega}$(gm) for an angular momentum **S** of a star or a torus. The following relation then applies to $\mathbf{\Omega}$(gm)

$$\frac{{\rm d}\mathbf{S}}{{\rm dt}} = \mathbf{\Omega}({\rm gm})\times\mathbf{S}. \tag{3.8}$$

The angular precession velocity $\mathbf{\Omega}$(gm) of **S** around direction of the field **B** from gravitomagnetic origin is given by [10, 12, 14]

$$\mathbf{\Omega}({\rm gm}) = -2\beta^{-1}c^{-1}G^{1/2}\mathbf{B}, \tag{3.9}$$

where the precession frequency ν(gm) is given by $\Omega({\rm gm}) = 2\pi\,\nu({\rm gm})$.

As a first example, the precession of the angular momentum $\mathbf{S}_{\rm m}$ of a circular torus with total mass $m_{\rm m}$ in the gravitomagnetic field of the star with angular momentum **S** will be considered. According to (3.8), an angular precession velocity $\mathbf{\Omega}$(gm) of the component $\mathbf{S}_{\rm m}\sin\delta_{\rm m}$ ($\delta_{\rm m}$ is the angle between the directions of **S** and $\mathbf{S}_{\rm m}$), perpendicular to **S**, occurs around **S**. An approximately equatorial orbit of the torus will be adopted (i.e., $\delta_{\rm m}$ is small). By substitution of the equatorial value of the gravitomagnetic field $\mathbf{B}_{\rm eq}$(gm) $= -R^{-3}\mathbf{M}$(gm) into (3.9) $\mathbf{\Omega}$(gm) can then directly be found

$$\mathbf{\Omega}_{\rm LT} = -c^{-2}GR^{-3}\mathbf{S}, \text{ or } \nu_{\rm LT} = -\tfrac{2}{5}c^{-2}Gm_{\rm s}\nu_{\rm s}r_{\rm s}^2R^{-3}. \tag{3.10}$$

The precession of the torus with mass $m_{\rm m}$ is an example of the Lense-Thirring precession of an orbital. Thus, the obtained result for $\mathbf{\Omega}$(gm) is denoted by $\mathbf{\Omega}_{\rm LT}$ and the corresponding Lense-Thirring frequency by $\nu_{\rm LT}$. It is noted, that $\mathbf{B}_{\rm eq}$(gm) is approximately constant, when $\delta_{\rm m}$ is small. Since $\mathbf{S}_{\rm m}\sin\delta_{\rm m}$ reduces to zero for $\delta_{\rm m}$ = 0, however, precession only occurs for $\delta_{\rm m} > 0$. In addition, it is noticed, that an ideal gravitomagnetic dipole moment **M**(gm), located at the centre of the star has been adopted in the derivation of (3.10). It has been shown in ref. [22], however, that for a homogeneous mass distribution in the sphere the equatorial value of the gravitomagnetic field $\mathbf{B}_{\rm eq}$(gm) at distance $R = r_{\rm s}$ may reduce to zero value. Then, according to (3.9), $\mathbf{\Omega}$(gm) = $\mathbf{\Omega}_{\rm LT}$ will also reduce to zero.

For $\delta_{\rm m}$ = 90º the gravitomagnetic field **B** in (3.9) is no constant and **B** has to be integrated over the whole orbit. An averaged result for the Lense-Thirring frequency $\overline{\nu_{\rm LT}}$ is then obtained for a circular orbit

$$\overline{\mathbf{\Omega}_{\rm LT}} = +2c^{-2}GR^{-3}\mathbf{S}, \text{ or } \overline{\nu_{\rm LT}} = \tfrac{4}{5}c^{-2}Gm_{\rm s}\nu_{\rm s}r_{\rm s}^2R^{-3}. \tag{3.11}$$

Note that both in the derivation of (3.10) and (3.11) a gravitomagnetic field **B** has been substituted into (3.9). For both cases it makes no difference, whether the field **B** is identified as a magnetic induction field (we do so) or not. Another situation occurs, when an electromagnetic field **B** = **B**(em) is substituted into (3.9). In section 4 we will consider examples of the latter alternative.

4. LOW FREQUENCY QUASI-PERIODIC OSCILLATIONS

If the field **B** in (3.9) may be identified with an electromagnetic field **B**(em), the following different gravitomagnetic precession frequencies can be distinguished (The adjective “gravitomagnetic” has been retained, since (3.9) describes the interaction

between some angular momentum and a magnetic field **B**). Substitution into (3.9) of the field **B**(em) from the outer torus with total charge Q_o and radius r_o, acting on the mass current with total mass m_m, yields a precession frequency ν_{mo}. The following sequence with respect to the subscripts has been used: the first subscript m in ν_{mo} stems from *middle* and the last subscript o from *outer*. The mass m_m in the torus with radius r_m in the *middle* experiences the action from the charge Q_o in the *outer* torus ($r_o > r_m$). Likewise, substitution into (3.9) of the field **B**(em) from the charge Q_i in the torus with radius r_i, acting on mass m_m, yields a frequency ν_{mi}. In addition, substitution of the field **B**(em) from charge Q_o, acting on the mass m_i in the torus with radius r_i and charge Q_i, yields a frequency ν_{io}. Further, substitution of the field **B**(em) from charge Q_i, acting on the mass m_o in the torus with radius r_o and charge Q_o, yields a frequency ν_{oi}. Thus, four new precession frequencies are obtained.

The derivation of the four precession frequencies has been given in ref. [10, sections 3 and 4]. Here we only give the results and some additional remarks. As a first example, the precession frequency ν_{mo} of the mass current with total mass m_m, due to the total charge Q_o in the torus with radius r_o, is given by

$$\nu_{mo} = -Q_o' \frac{2Gm_s}{c^2 r_o} \nu_o g(x_o) \cos\delta_m \cos\delta_o, \tag{4.1}$$

where Q_o' is again defined by $Q_o' \equiv (G^{½} m_s)^{-1} Q_o$. The frequency of the charge Q_o in the torus with radius r_o is given by ν_o (see (2.16)) and x_o is again defined by $x_o \equiv r_m/r_o$. In addition, δ_m and δ_o are the angles between the direction of the rotation axis of the star $\mathbf{s} = \boldsymbol{\Omega}_s/\Omega_s$ and the unit vectors $\mathbf{n}_m$ and $\mathbf{n}_o$ in the directions of the rotation axes of the tori with total mass m_m and total charge Q_o, respectively. The minus sign in (4.1) means that the angular precession velocity $\boldsymbol{\Omega}_{mo}$ ($\Omega_{mo} = 2\pi\nu_{mo}$) is counter-clockwise around $\mathbf{n}_o$ for $\beta = +1$ and a positive charge Q_o. The function $g(x_o)$ in (4.1) has been analogously defined to $g(x)$ in (2.19)

$$g(x_o) \equiv \frac{2}{\pi} \left\{ \frac{E(x_o)}{(1-x_o^2)} \right\}. \tag{4.2}$$

In addition, the charge Q_o in the outer torus with radius r_o acts on the mass m_i in the inner torus with radius r_i and may generate a precession frequency ν_{io}

$$\nu_{io} = -Q_o' \frac{2Gm_s}{c^2 r_o} \nu_o g(x) \cos\delta_i \cos\delta_o, \tag{4.3}$$

where Q_o', r_o, ν_o and δ_o are already given in (4.1) and x is again defined by $x \equiv r_i/r_o$. In addition, δ_i is the angle between the direction of the rotation axis of the star $\mathbf{s} = \boldsymbol{\Omega}_s/\Omega_s$ and the unit vector $\mathbf{n}_i$ in the direction of the rotation axis of the torus with mass m_i and charge Q_i. Note that the quantity $g(x)$ in (4.3) equals to $g(x)$ in (2.19).

Furthermore, the precession frequency ν_{mi} of the mass current with total mass m_m, due to the total electric charge Q_i in the torus with radius r_i, is given by

$$\nu_{mi} = Q_i' \frac{2Gm_s}{c^2 r_m} \nu_i x_i f(x_i) \cos\delta_m \cos\delta_i, \tag{4.4}$$

where Q_i' is again defined by $Q_i' \equiv (G^{½} m_s)^{-1} Q_i$. The frequency of the charge Q_i in the torus with radius r_i is given by ν_i (see (2.15)) and x_i is again defined by $x_i \equiv r_i/r_m$. The definitions of the angles δ_m and δ_i have already been given. The function $f(x_i)$ has analogously been defined to $f(x)$ in (2.9)

$$f(x_i) = \frac{-2}{\pi x_i}\left\{K(x_i) - \frac{E(x_i)}{1-x_i^2}\right\}. \tag{4.5}$$

Finally, the charge Q_i in the inner torus with radius r_i acts on the mass m_o in the outer torus with radius r_o and may generate a precession frequency ν_{oi}

$$\nu_{oi} = Q_i' \frac{2Gm_s}{c^2 r_o} \nu_i x f(x) \cos\delta_i \cos\delta_o, \tag{4.6}$$

where all parameters have already been given before. The quantity $f(x)$ has earlier been defined in (2.9).

Note that the four frequencies ν_{io}, ν_{mo}, ν_{oi} and ν_{mi} contain the dimensionless quantity $Gm_s/(c^2 r_o)$ or $Gm_s/(c^2 r_m)$. In general, the quantity $Gm_s/(c^2 r_o)$ is smaller than unity value for white dwarfs, pulsars and black holes, so that the frequencies ν_{mo} and ν_{io} are usually smaller than ν_o and may therefore be denoted as low frequency QPOs. An analogous line of reasoning can be applied to the frequencies ν_{mi} and ν_{oi}. Therefore, they can also be characterized as low frequency QPOs.

In addition, it is noticed that small angles δ_m, δ_o and δ_i have always been assumed in the derivations of the precession frequencies (4.1), (4.3), (4.4) and (4.6). If all values of δ nearly reduce to zero value, prograde motion of Q_i, m_m and Q_o around $\mathbf{s} = \boldsymbol{\Omega}_s/\Omega_s$ takes place. Alternatively, retrograde motion of Q_i, m_m and Q_o around $\mathbf{s}$ implies that all values of δ are about 180°.

Furthermore, a remark with respect to the relative magnitudes of ν_{mo} and ν_{io} can be made. Assuming $r_i < r_m < r_o$, implies $x_o > x$. According to table 1, the quantity $g(x_o)$ is then larger than $g(x)$. When the angles δ_m and δ_i do not differ too much, it follows from (4.1) and (4.3) that the frequency ν_{mo} is larger than ν_{io}. Finally, no sign of any of the frequencies ν_i, ν_m, ν_o, ν_{mo}, ν_{io}, ν_{mi} and ν_{oi} is known, at this moment. For that reason, positive signs for all frequencies will be used in the calculations below.

5. PARAMETER β^*

When both a magnetic induction field $\mathbf{B}_p$(gm) from gravitomagnetic origin and a field $\mathbf{B}_p$(em) from electromagnetic origin are present at, say, the north pole of the pulsar, the total magnetic induction field $\mathbf{B}_p$(tot) is given by

$$\mathbf{B}_p(\text{tot}) = \mathbf{B}_p(\text{gm}) + \mathbf{B}_p(\text{em}). \tag{5.1}$$

According to (3.6), the direction of $\mathbf{B}_p$(gm) is antiparallel to $\boldsymbol{\Omega}_s$ for $\beta = +1$. It appears helpful to define the following dimensionless quantity β^* (see ref. [13])

$$\mathbf{B}_p^{\square}(\text{tot}) = \beta^* \mathbf{B}_p(\text{gm}). \tag{5.2}$$

When the total field $\mathbf{B}$(tot) is from gravitomagnetic origin only, $\mathbf{B}_p$(em) = 0 and β^* reduces to $\beta^* = 1$. As a rule, measurements yield B_p(tot), so that only an estimate for β^* can be obtained.

Several contributions to the field $\mathbf{B}_p^{||}$(em) at the north pole of a star have been calculated in ref. [10]. First, a contribution $\mathbf{B}_p^{||}(\text{em}) = \mathbf{B}_p^{||}(Q_s)$ is generated by the charge Q_s in the star with radius r_s and rotational frequency ν_s. A second contribution $\mathbf{B}_p^{||}(\text{em}) = \mathbf{B}_p^{||}(Q_i)$ is generated by the charge Q_i moving in the circular torus with radius r_1. A third contribution $\mathbf{B}_p^{||}(Q_o)$ arises from charge Q_o moving in the circular torus with radius r_o.

Combination of the gravitomagnetic contribution of (3.6) with these contributions to $\mathbf{B}_p^{\parallel}$(em) leads to the following expression for the parameter β^* (see ref. [10])

$$\beta^* = 1 + \beta^*_{\text{current}} - Q_s' - \tfrac{5}{2} Q_i' \frac{\nu_i}{\nu_s} \frac{r_i^2/r_s^2 \cos\delta_i}{\left(1 + r_i^2/r_s^2\right)^{3/2}} - \tfrac{5}{2} Q_o' \frac{\nu_o}{\nu_s} \frac{r_o^2/r_s^2 \cos\delta_o}{\left(1 + r_o^2/r_s^2\right)^{3/2}}, \tag{5.3}$$

where δ_i is the angle between the direction of the rotation axis $\mathbf{s} = \boldsymbol{\Omega}_s/\Omega_s$ of the star and the unit vector $\mathbf{n}_i$, and so on. Quantities like Q_s' defined by $Q_s' \equiv (G^{1/2} m_s)^{-1} Q_s$ have been defined earlier. Note that the terms in Q_s', Q_i' and Q_o' are due to the contributions $\mathbf{B}_p^{\parallel}(Q_s)$, $\mathbf{B}_p^{\parallel}(Q_i)$ and $\mathbf{B}_p^{\parallel}(Q_o)$, respectively. The term β^*_{current} in (5.3) has been added to account for a possible contribution from toroidal currents in the star or black hole (see comment to (2.20)). For $\beta^*_{\text{current}} = -1$ toroidal currents completely compensate the magnetic field from gravitomagnetic origin. A striking property of (5.3) is that it provides a relation between the high frequency QPOs ν_o and ν_i, and the rotation frequency ν_s of the star. A related expression for β^* was previously deduced [13] for a star with a flat disk.

Since no stellar radius r_s has been defined for black holes, relation (5.3) cannot be applied in that case. A magnetic field $\mathbf{B}_p$(tot) at the poles of black holes is probably present, however. In order to obtain an estimate for β^*, r_s and ν_s in (5.3) are replaced by r_{out} from (1.5) for a chosen value of a, ϑ and Q_s', and by $\nu_s = c/(2\pi r_{\text{out}})$, respectively.

6. BLACK HOLES: THEORY AND OBSERVATIONS

In this section observations from the stellar black hole XTE J1550–564 and the supermassive black hole Sgr A* will be compared with predictions in previous sections. For that reason, the theoretical results will first be summarized.

6.1 Summary of theoretical results

The expressions for the frequencies ν_i from (2.15) and ν_o from (2.16) will only qualitatively be tested. In this work we will use the approximate relations (2.8) and (2.17)

$$Q_s \approx x^2 f(x)\, Q_o \quad \text{and} \quad Q_s \approx -g(x)\, Q_i, \tag{6.1}$$

where the quantity x is defined by $x \equiv r_i/r_o$. Instead of the quantities $f(x)$ and $g(x)$ in (6.1), the averaged values $\overline{f(x)} = \tfrac{1}{2}\{f_0 + f(x)\} = \tfrac{1}{2}\{0 + f(x)\} = \tfrac{1}{2} f(x)$ and $\overline{g(x)} = \tfrac{1}{2}\{g_0 + g(x)\}$ (see section 2) will be used in the calculations below.

The high frequency QPO ν_m has been given by (2.21)

$$\nu_m = \frac{1}{2\pi}\left(\frac{G m_s}{r_m^3}\right)^{1/2} \frac{1}{1 + \dfrac{S}{c^2 m_s}\left(\dfrac{G m_s}{r_m^3}\right)^{1/2}} = \frac{1}{2\pi}\left(\frac{G m_s}{r_m^3}\right)^{1/2} f_S. \tag{6.2}$$

This result applies for prograde motion of dm_m in the equatorial plane around a black hole. For white dwarfs and pulsars the relativistic factor f_S usually approaches unity, but for the black holes f_S may be smaller. When $S \to 0$, or $f_S \to 1$, one can write

$$r_K = \left\{\frac{G m_s}{\left(2\pi\nu_m\right)^2}\right\}^{1/3}. \tag{6.3}$$

An example of the more complicated relation (2.23) will be given in section 6.3.

The low frequency QPOs will be identified with the gravitomagnetic precession frequencies ν_{mo}, ν_{io}, ν_{mi} and ν_{oi} from (4.1), (4.3), (4.4) and (4.6) given by

$$\nu_{mo} = -Q_o' \frac{2Gm_s}{c^2 r_o} \nu_o \, g(x_o) \cos\delta_m \cos\delta_o, \quad x_o \equiv r_m/r_o, \tag{6.4}$$

$$\nu_{io} = -Q_o' \frac{2Gm_s}{c^2 r_o} \nu_o \, g(x) \cos\delta_i \cos\delta_o, \quad x \equiv r_i/r_o, \tag{6.5}$$

$$\nu_{mi} = Q_i' \frac{2Gm_s}{c^2 r_m} \nu_i \, x_i \, f(x_i) \cos\delta_m \cos\delta_i, \quad x_i \equiv r_i/r_m, \tag{6.6}$$

$$\nu_{oi} = Q_i' \frac{2Gm_s}{c^2 r_o} \nu_i \, x \, f(x) \cos\delta_i \cos\delta_o, \quad x \equiv r_i/r_o. \tag{6.7}$$

As an illustration, the precessing tori around the star with charge Q_i, mass m_m and charge Q_o, respectively, are schematically given in figure 3.

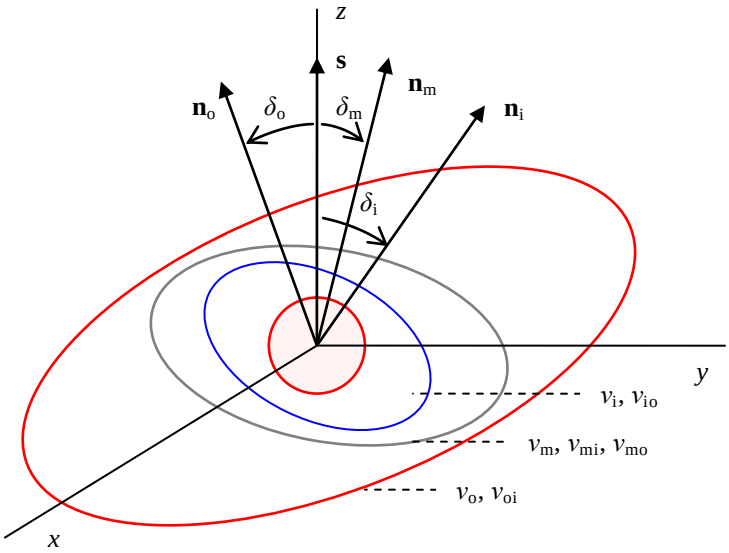

Figure 3. Rotation axes for a black hole or pulsar. The unit vector of the rotation axis of the star with charge Q_s (red) is $\mathbf{s} \equiv \boldsymbol{\Omega}_s/\Omega_s$. The unit vectors in the direction of the rotation axes of the circular tori with charge Q_i (blue), mass m_m (grey) and charge Q_o (red) are given by $\mathbf{n}_i$, $\mathbf{n}_m$ and $\mathbf{n}_o$, respectively. The angle between $\mathbf{s}$ and $\mathbf{n}_i$ is given by δ_i, and so on. The frequencies of the various tori are also denoted.

It is noticed that small angles δ_m, δ_o and δ_i (see figure 3) have been assumed in the derivations of the precession frequencies ν_{mo}, ν_{io}, ν_{mi} and ν_{oi}. If all values of δ nearly reduce to zero value, prograde motion of Q_i, m_m and Q_o around $\mathbf{s} = \boldsymbol{\Omega}_s/\Omega_s$ takes place. As a result of the precession processes, the angles δ (δ_o, δ_m and δ_i) occurring in (6.4)–(6.7) vary in time. When the angles δ are small, however, they may approximately be treated as constants in the derivations of (5.3) and (6.4)–(6.7). Since all angles δ occur as $\cos\delta$ in these equations, the introduced errors are small in that case. Furthermore, it will be assumed that $r_i < r_m < r_o$.

In favourable cases the mass m_s, the radius r_s and seven frequencies (i.e., ν_o, ν_m, ν_i, ν_{mo}, ν_{io}, ν_{mi} and ν_{oi}) are known. Nine unknown quantities are to be found (i.e., three charges: Q_s, Q_o and Q_i; three radii: r_o, r_m and r_i; three angles: δ_o, δ_m and δ_i). Only the parameter r_K can directly be calculated from (6.3), when the frequency ν_m can be assigned and when $\nu_m \approx \nu_k$. Only seven relations are available (i.e., two from (6.1), one from (6.3)

and four from (6.4)–(6.7)). Therefore, we have arbitrarily chosen one δ value, e.g., δ_m, and we have adopted $\delta_i = \delta_o$. Thus, choosing the value of two parameters, it appears possible to calculate the values of the remaining seven unknown quantities.

It is noted that by combining (6.1), (6.5) and (6.7) the following relation can be obtained, independent of $\cos\delta_i$, $\cos\delta_o$, Q_s, Q_o and Q_i

$$\frac{\nu_{io}\nu_i}{\nu_{oi}\nu_o} = \frac{g(x)^2}{x^3 f(x)^2}. \tag{6.8}$$

It appears that all parameters x, $f(x)$ (or $\overline{f(x)}$) and $g(x)$ (or $\overline{g(x)}$) on the right hand side of (6.8) only depend on x. When all frequencies on the left hand side of (6.8) are known, all parameters on the right hand side can separately be calculated by an iteration process. In the calculations below use has been made of relation (6.8).

6.2 Stellar black hole XTE J1550–564

It is generally assumed that the *binary* system XTE J1550–564 contains a stellar black hole. As has previously been discussed [10], seven QPO frequencies may be extracted from observations (compare with a set of five QPO frequencies considered in ref. [8]). The seven QPO frequencies have been assigned to ν_i, ν_m, ν_o, ν_{mo}, ν_{io}, ν_{mi} and ν_{oi}, respectively (see our table 2). Keeping in mind the assumption $r_i < r_m < r_o$ in our model, the highest frequencies are attributed to ν_i, ν_m and ν_o, respectively. An estimate of the relative magnitudes of the other four frequencies can often be made. For example, the frequency ν_{mo} is usually larger than ν_{io}, as has been discussed in section 4.

Introduction of the values $m_s = 9.61\ m_\odot$ and $\nu_m = \nu_K = 188$ Hz (see table 2) for XTE J1550–564 into (6.3) yields for the Kepler radius $r_K = 9.706\times10^6$cm $= 6.838 r_g$ ($r_g \equiv Gm_s/c^2 = 1.419\times10^6$cm). In fact, we then assume a non-rotating black hole with angular momentum $S = 0$, so that $f_S = 1$ (see (6.2)). Alternatively, the extreme value $S = cm_s r_g$ may be assumed for XTE J1550–564, resulting into

$$S = cm_s a = cm_s r_g = \frac{Gm_s^2}{c} = 8.134\times10^{50}\,\mathrm{g.cm^2.s^{-1}}. \tag{6.9}$$

Substitution of the parameters $m_s = 9.61\ m_\odot$, $\nu_m = 188$ Hz and the extreme value S from (6.9) into (6.2) yields $r_m = 9.340\times10^6$cm $= 6.580 r_g$ and $f_S = 0.7195$.

In addition, the parameters x, $\overline{f(x)}$ and $\overline{g(x)}$ have been calculated from (6.8) by an iteration process (see comment to this relation). Precise values of these parameters have been given in table 2, since these quantities are often very sensitive to small mutual changes in their value. Of course, the real accuracy of these parameters is much more limited. Note that the parameters x, $\overline{f(x)}$ and $\overline{g(x)}$, can be calculated from (6.8) without knowledge of the value of mass m_s.

In the next step, frequencies ν_i and ν_o from table 2, m_s and the calculated parameters x, $\overline{f(x)}$, $\overline{g(x)}$ are combined with equations (6.1), (6.4)–(6.7). In addition, a value for $\delta_m = 5^o$ and the approximation $\delta_i = \delta_o$ is chosen. By application of an additional iteration process, accurate fits could then be found between observed and calculated values of ν_{mo}, ν_{io}, ν_{mi} and ν_{oi}. Precise values for the obtained parameters x_i, $\overline{f(x_i)}$, $\overline{g(x_i)}$, x_o, $\overline{f(x_o)}$, $\overline{g(x_o)}$, Q_s', Q_o', Q_i', r_K, r_m, δ_i, δ_m and δ_o have been summarized in table 2. It is stressed again that the real accuracy of all these parameters is much more limited, especially the δ values. Results for XTE J1550–564 given in ref. [10] are based on r_K, but the results presented in table 2 are based on the value of r_m. Note that the parameters x, $\overline{f(x)}$, $\overline{g(x)}$, x_i, $\overline{f(x_i)}$, $\overline{g(x_i)}$, x_o, $\overline{f(x_o)}$, $\overline{g(x_o)}$ and δ are not affected by this change.

Table 2. QPO frequencies ν_0 (so-called centroid frequencies), values of the half-width signal at half maximum Δ, quality factors Q defined by $Q \equiv \nu_0/(2\Delta)$, integrated fractional r.m.s. amplitudes and calculated parameters for black hole XTE J1550–564. The calculated parameters are: relative radii (x, x_o and x_i), radii (r_i, r_m and r_o), relative charges Q_s', Q_o' and $-Q_i'$ (Q' is defined by $Q' \equiv (G^{1/2}m_s)^{-1}Q$), factors $\overline{f(x)}$, $\overline{g(x)}$, $\overline{f(x_i)}$, $\overline{g(x_i)}$, $\overline{f(x_o)}$ and $\overline{g(x_o)}$ and angles δ_i and δ_o. See text for comment.

ν_0[a] (Hz)	Δ[a] (Hz)	Q[a]	r.m.s.[a] (%)	x	$R\times10^6$ (cm)	Q'	$\overline{f(x)}$[b]	$\overline{g(x)}$[b]	δ (^{o})
ν_s ?						Q_s' 0.0971			
ν_i 268	56	2.4	6.2		r_i 8.262	$-Q_i'$ 0.0677			δ_i 43.97
ν_m 188	24	3.9	2.8		r_m 9.340	Q' 0			δ_m 5
ν_o 62.9	9.4	3.3	8.7		r_o 11.32	Q_o' 0.4298			δ_o 43.97
ν_{mo} 8.75			5.8	x_o 0.82532	r_o 11.32	Q_o' 0.4298		$\overline{g(x_o)}$ 1.7997	$\delta_m=5$, δ_o
ν_{io} 5.04			16.4	x 0.73000	r_o 11.32	Q_o' 0.4298		$\overline{g(x)}$ 1.4348	$\delta_i=\delta_o$ 43.97
ν_{mi} 4.090	0.72	2.8	10.4	x_i 0.88451	r_m 9.340	$-Q_i'$ 0.0677	$\overline{f(x_i)}$ 1.1695		$\delta_m=5$, δ_i
ν_{oi} 0.73			10.1	x 0.73000	r_o 11.32	$-Q_i'$ 0.0677	$\overline{f(x)}$ 0.4241		$\delta_i=\delta_o$ 43.97

[a] See ref. [10] and references therein. [b] Definitions of these quantities have been given in sections 2 and 4.

Table 2 shows that the obtained values for δ_i and δ_o are not small. In the derivations of the expressions ν_{io} and ν_{oi}, however, small values for δ_i and δ_o have been adopted. In addition, line charges Q_i and Q_o in two tori have been assumed. However, when the charges Q_i and Q_o reside in an inner and outer belt, respectively, the system may be more stable. The belts could be compared with the observed inner and outer Van Allen radiation belts around the Earth. Thus, the results of table 2 may remain approximately valid.

Instead of the identifications of table 2, one might choose: ν_i = 268 Hz, ν_o = 62.9 Hz, ν_{oi} = 5.04 Hz and ν_{io} = 0.73 Hz. Substitution of these frequencies in the left hand side of (6.8), however, yields a result smaller than unity value, incompatible with the prediction of the right hand side. Therefore, this alternative choice must be rejected.

Since the values of the parameter β^* and the rotation frequency ν_s are unknown for XTE J1550–564, no value of β^*_{current} for XTE J1550–564 can be calculated from (5.3). Furthermore, a stellar radius r_s has not been defined for a black hole, so that the Lense-Thirring precession frequency ν_{LT} from (3.10b) cannot be calculated. Combination of (3.10a), the angular momentum S from (6.9) and radius $R = r_i$ from table 2, however, yields $\nu_{LT}(m_i)$ = 17.0 Hz for the Lense-Thirring precession frequency of the inner torus with mass m_i. Since S may be smaller than the extreme value $S = cm_sr_g$, this value for $\nu_{LT}(m_i)$ may also be smaller. Moreover, the equatorial value of the gravitomagnetic field $\mathbf{B}_{eq}$(gm) at distance $R = r_i$ may be smaller than assumed, also resulting into a smaller value for $\nu_{LT}(m_i)$ (see comment to (3.10)).

It is noticed that the opposite sign of *all* charges of Q_s, Q_i and Q_o given in table 2 is also compatible with the same set of parameters x, r, δ, $\overline{f(x)}$ and $\overline{g(x)}$ in that table.

Finally, it is noted that the Kepler radius of 7.66×10^6cm = $5.40\,r_g$ calculated from ν_i is smaller than the innermost stable circular orbit in Schwarzschild space-time $r_{ISCO} = 6r_g$. For $a = 0$ and $Q_s' = 0.1009$ in Reissner-Nordstrøm space-time, however, a value of $r_{ISCO} = 5.98\,r_g$ is obtained from (1.6), compatible with the value $r_i = 8.585\times10^6$cm = $6.05\,r_g$

deduced in ref. [10]. For $a = r_g$ and $Q_s' = 0.0971$ in Kerr-Newman space-time, a stable circular orbit of radius $r_i = 8.262\times10^6$ cm $= 5.82\, r_g$ follows from (1.6) ($F > 0$). See table 2. No preference value for a can be extracted for XTE J1550–564 from our model.

6.3 Galactic black hole Sgr A*

For the supermassive black hole Sgr A* in the Galactic Center Miyoshi *et al.* [2] detected radio emissions in 2004, using the *Very Long Baseline Array* (*VLBA*). From their analysis of the data they obtained seven different QPO periods. All these periods and the corresponding frequencies are summarized in our table 3. Previously, Aschenbach *et al.* [3] reported more than seven QPO frequencies from two X-ray flares of Sgr A*, detected by *Chandra* in 2000 and by *XMM-Newton* in 2002. In addition, a number of QPO frequencies was covered by *IR* measurements (see ref. [3, especially table 2]). A review of the observations of Sgr A* up to about of 2005 was given by Aschenbach [4]. He concluded, that recent measurements gave no confirmation for QPO frequencies higher than about 1.5 mHz. Since the results of Miyoshi *et al.* [2] are less ambiguous, these data are used in our calculations. As can be seen from our table 3, a set of seven QPO frequencies may be assigned to the frequencies ν_i, ν_m, ν_o, ν_{mo}, ν_{io}, ν_{mi} and ν_{oi}.

For a non-rotating black hole the Kepler radius r_K can again be calculated from (6.3) by introduction of the value $m_s = 3.7\times10^6 m_\odot$, reported by Ghez *et al.* [15], and the *VLBA* value $\nu_K = 0.992$ mHz. One obtains $r_K = 2.330\times10^{12}$ cm $= 4.263\, r_g$ (see also (1.1)). According to (6.2), in that case $S = 0$ and $f_S = 1$. Alternatively, in extreme Kerr space-time substitution of the same value of m_s, $\nu_m = 0.992$ mHz and the extreme value $S = c\, m_s\, r_g$ from (3.4) into (6.2) yields $r_m = 2.150\times10^{12}$ cm $= 3.933\, r_g$ and $f_S = 0.8864$.

Table 3. QPO periods (P) and QPO frequencies (ν) of the supermassive black hole Sgr A* from *Very Long Baseline Array* observations. See caption of table 2 for further comment.

P[a] (min)	ν[a] (mHz)	x	$R\times10^{12}$ (cm)	Q'	$\overline{f(x)}$[b]	$\overline{g(x)}$[b]	δ (°)
P_s ?	ν_s ?			Q_s' 0.2907			
P_i 12.9	ν_i 1.29		r_i 1.959	$-Q_i'$ 0.1465			δ_i 16.35
P_m 16.8	ν_m 0.992		r_m 2.150	Q' 0	$\overline{f(x_o)}$ 2.209	$\overline{g(x_i)}$ 2.769	δ_m 10
P_o 22.2	ν_o 0.751		r_o 2.299	Q_o' 0.4536			δ_o 16.35
P_{mo} 31.4	ν_{mo} 0.531	x_o 0.93511	r_o 2.299	Q_o' 0.4536		$\overline{g(x_o)}$ 3.469	δ_m=10 δ_o=16.35
P_{io} 56.4	ν_{io} 0.296	x 0.85224	r_o 2.299	Q_o' 0.4536		$\overline{g(x)}$ 1.985	δ_i= δ_o= 16.35
P_{mi} 128.4	ν_{mi} 0.130	x_i 0.91137	r_m 2.150	$-Q_i'$ 0.1465	$\overline{f(x_i)}$ 1.571		δ_m=10 δ_i=16.35
P_{oi} 268	ν_{oi} 0.0622	x 0.85224	r_o 2.299	$-Q_i'$ 0.1465	$\overline{f(x)}$ 0.8824		δ_i= δ_o= 16.35

[a] Ref. [2]. [b] Definitions of these quantities have been given in sections 2 and 4.

In addition, the parameters x, $\overline{f(x)}$) and $\overline{g(x)}$ can be calculated from (6.8) by the same method applied in section 6.2. In the next step, the frequency $\nu_i = 1.29$ mHz from *VLBA* observations, the frequency $\nu_o = 0.751$ mHz from X-ray flares (see table 3), $m_s = 3.7\times10^6\ m_\odot$, and the calculated parameters x, $\overline{f(x)}$, $\overline{g(x)}$, are combined with equations (6.1), (6.4)–(6.7). In addition, a value for $\delta_m = 10^o$ and the approximation $\delta_i = \delta_o$ is chosen. By application of an iteration process, accurate fits could then be found between

observed *VLBA* values of ν_{mo} = 0.531 mHz, ν_{io} = 0.296 mHz, ν_{mi} = 0.130 mHz, ν_{oi} = 0.0622 mHz and the corresponding calculated values. Precise values for the obtained parameters for x_i, $\overline{f(x_i)}$, $\overline{g(x_i)}$, x_o, $\overline{f(x_o)}$, $\overline{g(x_o)}$, Q_s', Q_o', Q_i', r_K, r_m, δ_i, δ_m and δ_o have been summarized in table 3. It is stressed again that the real accuracy of the parameters is much more limited. Results for Sgr A* presented in table 3 are based on the value of r_m. When the calculations are based on the value of r_K, however, the parameters x, $\overline{f(x)}$, $\overline{g(x)}$, x_i, $\overline{f(x_i)}$, $\overline{g(x_i)}$, x_o, $\overline{f(x_o)}$, $\overline{g(x_o)}$ and δ do not change.

As an alternative for the assignments in table 3, one may try: ν_i = 1.29 mHz, ν_o = 0.751 mHz, ν_{oi} = 0.296 mHz and ν_{io} = 0.0622 mHz. Substitution of these frequencies in the left hand side of (6.8), however, yields a result smaller than unity value, incompatible the prediction of the right hand side. Therefore, this alternative choice must be rejected.

Contrary to most pulsars, the velocity of a point charge in a circular orbit around the supermassive black hole like Sgr A* may closely approach the light velocity c. As an example, we will compare the velocity v_i of a charge element dQ_i of the inner torus with c. Choosing ν_i = 1.29 mHz and $r_i = 1.959\times10^{12}$cm = $3.585\,r_g$ from relation $r_i = x_i\, r_m$ (see table 3), one obtains

$$\frac{v_i}{c} = \frac{2\pi\nu_i r_i}{c} = 0.53. \tag{6.10}$$

This result for r_i can also be compared with the corresponding Kepler radius $r_K = \{Gm_s/(2\pi\nu_i)^2\}^{1/3} = 1.955\times10^{12}$cm = $3.578\,r_g$. The latter value suggests that the charge dependent contribution to the right hand side of (2.15) is rather small in this case (see also comment to (2.15)).

From $r_K = 2.330\times10^{12}$cm = $4.263\,r_g$ and relation $r_i = x_i\, r_K$ it follows that $r_i = 2.123\times10^{12}$cm = $3.885\,r_g$. This value for r_i is incompatible with the innermost stable circular orbit $r_{ISCO} = 5.85\,r_g$ in Reissner-Nordstrøm space-time, calculated from (1.6) for the values a = 0 and Q_s' = 0.3150. Analogously, choosing a value $a = r_g$, radius r_i can be calculated from $r_m = 2.150\times10^{12}$cm = $3.933\,r_g$, resulting into $r_i = x_i\, r_m = 1.959\times10^{12}$cm = $3.585\,r_g$. From (1.6) follows that the circular orbit for $r_i = 3.585\,r_g$, $a = r_g$ and Q_s' = 0.2907 is stable ($F > 0$). Moreover, assuming $r_i = r_{ISCO}$, it appears possible to find a unique value for the ratio a/r_g by combination of the relations (1.6) for F = 0, (6.2) and $r_i = x_i\, r_m$. Application of the iteration process yields: a/r_g = + 0.584 for $r_m = 4.072\,r_g$, $r_i = 3.711\,r_g$ and Q_s' = 0.3009. The latter value of r_i can be compared with the equatorial radius $r_{out} = 1.954\,r_g$ from (1.5) for $a = +\,0.584\,r_g$, $\vartheta = 90^o$ and Q_s' = 0.3009.

Calculations above illustrate, that frequencies ν_m obtained from (2.21) for a non-zero angular momentum S differ from the Kepler frequency ν_K. Another modification of ν_K occurs, when the *gravitational* attractions between the torus with mass m_m and masses m_i and m_o in the other tori are taken into account. Calculation shows, that the frequency ν_m for a mass element dm_m in the torus with total mass m_m is then given by (2.23). Although the values for $\overline{f(x_o)}$ and $\overline{g(x_i)}$ have been calculated (see table 3), the values of the masses m_i, m_m and m_o are not known. However, since m_i and m_o are probably much smaller than m_s, the terms in (2.23) depending on m_i and m_o can be neglected and ν_m reduces to the Kepler frequency ν_K.

As has been discussed in section 3, our interpretation of the gravitomagnetic field leads to a prediction of a magnetic field B_p(gm) at the poles of the black hole. For example, for the choices $a = r_g$, $\vartheta = 0^o$ and Q_s' = 0 (extreme Kerr space-time), one obtains $r_{out} = r_g$ from (1.5) for the distance from the centre of the black hole to a pole. Assuming $\beta = +\,1$, a value B_p(gm) = $-\,6.4\times10^{12}$G is found in (3.7). When the values $a = +\,0.584\,r_g$, $\vartheta = 0^o$ and Q_s' = 0.3009 are substituted into (1.5), one finds $r_{out} = 1.75\,r_g$ in the more general Kerr-Newman space-time. Assuming again $\beta = +\,1$, a value B_p(gm) = $-\,6.9\times10^{11}$G can then be calculated from a combination of (3.1), (3.3), (3.5) and $R = r_{out} = 1.75\,r_g$. No

reliable value for the total field B_p(tot) at the poles of the black hole from (5.1) is known, but the field of Sgr A* may be much lower than B_p(gm).

In order to deduce an estimate for the parameter β^* in (5.3) for Sgr A*, we will replace radius r_s by the equatorial radius $r_{out} = 1.954 r_g$ from (1.5) for $a = +0.584 r_g$, $\vartheta = 90^o$ and $Q_s' = +0.3009$. For the values of Q_i' and Q_o', corresponding to Q_s', one finds: $Q_i' = -0.1516$ and $Q_o' = +0.4695$. In addition, we approximate ν_s by $\nu_s = c/(2\pi r_{out}) = 4.47$ mHz by utilizing the equatorial radius $r_{out} = 1.954 r_g$. Calculation then yields the following result for the parameter β^* (see table 3 for additional parameters)

$$\beta^* = 1 + \beta^*_{current} - 0.301(\text{from } Q_s) + 0.038(\text{from } Q_i) - 0.065(\text{from } Q_o). \qquad (6.11)$$

Note that the contributions from the tori with charges Q_i and Q_o to $B_p^{||}$(tot) are small and almost cancel.

As has previously been discussed [10], the parameter β^* in (5.3) may be small for fast rotating pulsars. Assuming $\beta^* \approx 0$ for Sgr A* in (6.11), leads to the value $\beta^*_{current} \approx -0.67$. This result implies that toroidal currents may largely compensate the magnetic field from gravitomagnetic origin. Note that for the fast rotating pulsars XTE J1807–294, IGR J00291+5934 and SAX J1808.4–3658 comparable values for $\beta^*_{current}$ were found [10]: – 0.737, – 0.563 and – 0.499, respectively.

It is noticed that the opposite sign of *all* charges of Q_s, Q_i and Q_o given in table 3 is compatible with the same set of parameters x, r, δ, $\overline{f(x)}$ and $\overline{g(x)}$ in those tables. The choice of the opposite the sign of all charges, however, leads to a value $\beta^*_{current} \approx -1.33$ for Sgr A*.

Since no rotation frequency ν_s is known for Sgr A* and no stellar radius r_s has been defined for a black hole, the Lense-Thirring precession frequency ν_{LT} from (3.10b) cannot be calculated. Combination of (3.10a), the angular momentum S for $a = 0.584 r_g$ from (3.3) and radius $R = r_i = 3.711 r_g$, however, yields the result $\nu_{LT}(m_i) = 0.100$ mHz for the Lense-Thirring precession of the inner torus with mass m_i. Since the orbit of this torus is close to the equatorial radius $r_{out} = 1.954 r_g$, the magnetic dipole approximation for the black hole is no longer valid and the value of $\nu_{LT}(m_i)$ will become smaller (see ref. [22] and comment to (3.10)).

Finally, it is has been suggested by Ballantyne *et al*. [23] that Sgr A* may be a source protons with an energy of several TeV. The present model may explain their origin: the protons due to the charge Q_s may leave the black hole at the poles during expansion of the outer torus with charge Q_o. In addition, protons may escape at the equator from the outer torus. Compare with comment to equation (2.20).

7. MASS OF SGR A*

In view of its importance with respect to this and other work the value of the mass of Sgr A* is considered more in detail in this section. From 17 proper-motion stars near the Galactic Center Ghez, Salim, Hornstein *et al.* [15] calculated a central mass of $(3.7 \pm 0.2)\times 10^6 m_\odot$ for a distance $R_0 = 8$ kpc. In addition, Ghez, Salim, Weinberg *et al.* [16] analyzed the Keplerian orbit of the short period star S0-2, and deduced a value of $(4.1 \pm 0.6)\times 10^6 m_\odot$ for the enclosed mass at distance $R_0 = 8.0 \pm 0.6$ kpc (both quoted uncertainties are 68% confidence values). Moreover, they concluded from complex models, that the extended mass distribution amounts to less than $3\text{-}4\times 10^5 m_\odot$ within 0.01 pc. Furthermore, Schödel, Merrit and Eckart [17] measured the proper motions of more than 6000 stars and deduced a best-fit black hole mass of $(3.6 + 0.2/-0.4)\times 10^6 m_\odot$. In this work, a value $m_s = 3.7\times 10^6 m_\odot$ for the supermassive black hole Sgr A* has been used.

In this section we derive new expressions for the effective mass m_s(eff) of a black hole acting on a companion star of mass m_c ($m_c << m_s$), moving in a circular orbit around that black hole. It is assumed that an additional massive torus is present, also moving in a

circular orbit around the black hole. It appears that the calculated effective mass m_s(eff) depends on the mass and the orientation of the orbital plane of the torus. Two expressions are deduced: one for coinciding orbital planes of companion star and torus and one for perpendicular orbital planes. Results are qualitatively compared with the reported mass value for Sgr A*, deduced from the orbit of the companion star S0-2.

More in detail, we first consider a binary system, consisting of a black hole with mass m_s and a companion star with mass m_c, moving in a circular orbit of radius r_c around the black hole. In addition, an inner torus with radius r_i and mass m_i and an outer torus with radius r_o and mass m_o are assumed to move in a circular orbits around the same black hole. The unit rotation vector $\mathbf{n}_c$ of the orbit of the companion star and the unit vectors $\mathbf{n}_i$ and $\mathbf{n}_o$ of the orbits of the tori with mass m_i and mass m_o, respectively, all coincide. This configuration will be denoted as system A.

Analogous to the calculation of the Coulomb forces of $\mathbf{F}_{is}$ of (2.7), $\mathbf{F}_{oi}$ of (2.17) (from ref. [10]) and $\mathbf{F}_{io}$ of (2.4), the Newtonian forces between black hole with mass m_s and the star with mass m_c, $\mathbf{F}_{cs}$, between mass m_c and torus with mass m_i, $\mathbf{F}_{ci}$, and between mass m_c and torus with mass m_o, $\mathbf{F}_{co}$ can be calculated. One obtains for system A

$$\mathbf{F}_{cs} = -\frac{Gm_c m_s}{r_c^2}\mathbf{i}_c, \quad \mathbf{F}_{ci} = -g(x_i)\frac{Gm_c m_i}{r_c^2}\mathbf{i}_i \quad \text{and} \quad \mathbf{F}_{co} = f(x_o)\frac{Gm_c m_o}{r_o^2}\mathbf{i}_o, \tag{7.1}$$

where x_i is defined by $x_i \equiv r_i/r_c$ and x_o by $x_o \equiv r_c/r_o$. In addition, the unit vector $\mathbf{i}_c$ is given by $\mathbf{i}_c = \mathbf{r}_c/|\mathbf{r}_c|$, and so on. The spherical coordinate θ between the unit vector $\mathbf{n}_c$ and the orbital planes of both tori is 90º. In addition, the quantities $f(x_o)$ and $g(x_i)$ are analogously defined to (2.24). The total gravitational force, $\mathbf{F}_{cs}$(tot), acting on mass m_c, is then given by

$$\mathbf{F}_{cs}(\text{tot}) = \mathbf{F}_{cs} + \mathbf{F}_{ci} + \mathbf{F}_{co} = -\frac{Gm_c m_s}{r_c^2}\mathbf{i}_c\left(1 + g(x_i)\frac{m_i}{m_s} - f(x_o)x_o^2\frac{m_o}{m_s}\right). \tag{7.2}$$

Comparison of the forces $\mathbf{F}_{cs}$ in (7.1) and $\mathbf{F}_{cs}$(tot) in (7.2) shows, that the companion star with mass m_c is subjected to the Newtonian force from an effective mass $m_s^{\parallel}$(eff) of magnitude

$$m_s^{\parallel}(\text{eff}) = m_s + g(x_i)m_i - x_o^2 f(x_o)m_o = m_s + \Delta m^{\parallel}. \tag{7.3}$$

The superscript $\parallel$ has been added, since the directions of all unit rotation vectors $\mathbf{n}_c$, $\mathbf{n}_i$ and $\mathbf{n}_o$ of the orbits of masses m_c, m_i, and m_o, respectively, coincide. Note that the value of $m_s^{\parallel}$(eff) is enhanced by the torus with mass m_i, whereas it is diminished by the torus with mass m_o (see also table 1).

Two limiting cases of (7.3) will now be distinguished. First, when $m_o = 0$ and x_i approaches to zero value, $g(x_i)$ approaches to unity value (see table 1). In this case, $m_s^{\parallel}$(eff) approaches to the value $m_s^{\parallel}$(eff) = $m_s + m_i$. Such a result must be expected, because the companion star is subjected to the gravitational attraction of the black hole mass m_s plus mass m_i. Secondly, when relations $x_i = x_o \equiv x$ and $m_i = m_o \equiv m$ apply, the following values for $\Delta m^{\parallel}$ can be calculated from table 1

$$\begin{aligned} &x = 0.99670 \rightarrow \Delta m^{\parallel} = 2.799\,m, \quad x = 0.94449 \rightarrow \Delta m^{\parallel} = 1.893\,m, \\ &x = 0.71543 \rightarrow \Delta m^{\parallel} = 1.348\,m, \quad x = 0.49903 \rightarrow \Delta m^{\parallel} = 1.159\,m. \end{aligned} \tag{7.4}$$

From (7.3) and (7.4) follows, that for, e.g., $x = 0.99670$ the companion star is attracted by a total mass $m_s + m$ enclosed by its orbit, plus an additional mass contribution of 1.799 m. This effect is caused by the short distances between the companion star and both tori.

Alternatively, an effective mass $m_s^{\perp}(\text{eff})$ can be calculated for another configuration of the same components, denoted as system B. In this system the rotation unit vector $\mathbf{n}_c$ of the orbit of the companion star with mass m_c is perpendicular to the coinciding unit rotation vectors $\mathbf{n}_i$ and $\mathbf{n}_o$ of the orbits of the tori with mass m_i and mass m_o, respectively. System B is schematically given in figure 4.

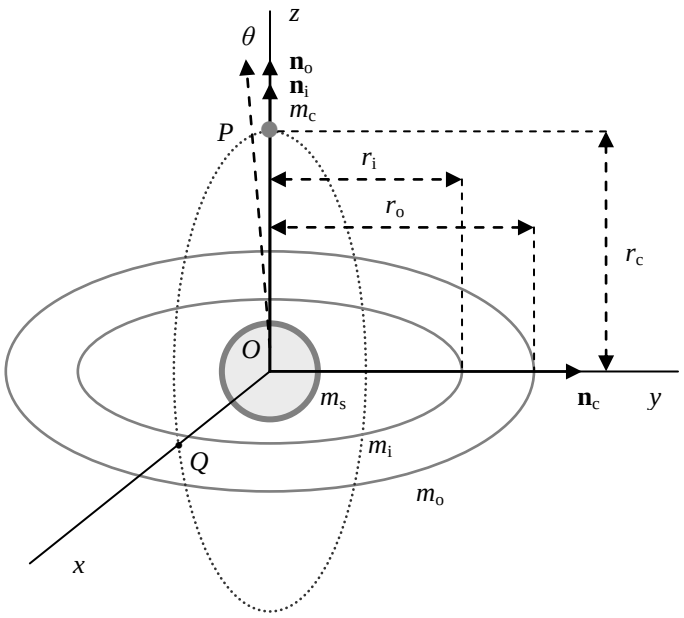

Figure 4. Configuration of system B. The vector $\mathbf{n}_c$ denotes the unit rotation vector perpendicular to the orbit of the companion star with mass m_c. The unit rotation vectors $\mathbf{n}_i$ and $\mathbf{n}_o$ of the orbits of the tori with mass m_i and mass m_o, respectively, coincide with the z axis. The spherical coordinate θ, the angle between OP (O is the centre of the black hole and P is the position of the companion star) and the vectors $\mathbf{n}_i$ and $\mathbf{n}_o$ is given by $\theta = 0^o$. Point Q (with $\theta = 90^o$) is another position of the orbit of the companion star, discussed in the text. Note that in this derivation the unit vector $\mathbf{s} \equiv \mathbf{\Omega}_s/\Omega_s$ along the rotation axis of the black hole with mass m_s star need not to be specified.

Using again the formalism of section 2, the total Newtonian force from black hole and both tori acting on the companion star can be calculated. The position P of the latter star is characterized by the spherical coordinate $\theta = 0^o$ (see figure 4). An expression for $m_s^{\perp}(\text{eff})$, analogous to (7.3) can be found. Substitution of the quantities $g(x_i)$ from (2.22) in ref. [10] and $f(x_o)$ from (2.12) in this work, respectively, yields the following expression for $m_s^{\perp}(\text{eff})$

$$m_s^{\perp}(\text{eff}) = m_s + \frac{m_i}{\left(1+x_i^2\right)^{3/2}} + \frac{x_o^3\, m_o}{\left(1+x_o^2\right)^{3/2}} = m_s + \Delta m^{\perp}, \tag{7.5}$$

where x_i is again defined by $x_i \equiv r_i/r_c$ and x_o by $x_o \equiv r_c/r_o$. Note that the value of $m_s^{\perp}(\text{eff})$ in (7.5) increases by the contribution of both inner and outer torus.

When $m_o = 0$ and x_i approaches to zero value, $m_s^{\perp}(\text{eff})$ also approaches to the limiting value $m_s^{\perp}(\text{eff}) = m_s + m_i$, equal to the result of (7.3) in the corresponding limiting case. Choosing $x_i = x_o \equiv x$ and $m_i = m_o \equiv m$ as a second limiting case, the following values for $\Delta m^{\perp}$ can be calculated from table 1

$$x = 0.99670 \rightarrow \Delta m^{\perp} = 0.707\, m, \quad x = 0.94449 \rightarrow \Delta m^{\perp} = 0.708 m,$$
$$x = 0.71543 \rightarrow \Delta m^{\perp} = 0.735\, m, \quad x = 0.49903 \rightarrow \Delta m^{\perp} = 0.805\, m. \tag{7.6}$$

The different values for $\Delta m^{\parallel}$ from (7.4) and $\Delta m^{\perp}$ from (7.6) imply different values for the effective masses $m_s^{\parallel}$(eff) and $m_s^{\perp}$(eff) (see (7.3) and (7.5), respectively). Thus, the orientation of a torus or disk will cause an *anisotropy* in the value of the effective mass m_s(eff) of the black hole. A related anisotropy has been proposed by Schödel, Merrit and Eckart [17] in their analysis of proper motions of stars orbiting around Sgr A*. As shown above, when $m_o = 0$ and x_i approaches to zero value, both $m_s^{\parallel}$(eff) and $m_s^{\perp}$(eff) reduce to m_s plus m_i. In this limiting case the effective mass m_s(eff) of the black hole is *isotropic*.

The results of (7.4) and (7.6) lead to another remarkable prediction. To that end, consider the circular orbit of the companion star in system B, as illustrated in figure 4. As an example, for an arbitrarily chosen value like $x = 0.99670$, the latter star is subjected to an effective mass $m_s^{\perp}$(eff) = m_s + 0.707 m (see (7.5) and (7.6)) in point P and an effective mass $m_s^{\parallel}$(eff) = m_s + 2.799 m (see (7.3) and (7.4)) in point Q of its orbit (see figure 4). As a result, the initially circular orbit of the companion star around the black hole will become approximately elliptical with, e.g., Sgr A* located *in the centre* of the ellipse (*not in a focal point!*). Note that the described effect does not occur for the configuration of system A. In the latter case the value of the effective mass m_s(eff) is constant along the whole orbit of the companion star.

In order to compare the described new effect with observations, the companion star S0-2 orbiting around Sgr A* may be considered. Assuming an ellipsoidal, Keplerian orbit for the star S0-2, Ghez, Salim, Weinberg *et al.* [16]) indeed found a small tentative difference between the focal point of the star and the position of the black hole. Before more definite conclusions can be drawn, however, more data about mass value, orientation and location of a massive torus or disk should be known.

Considering system A and utilizing (7.3) and (7.4), an estimate for the effective mass $m_s^{\parallel}$(eff) of Sgr A* may be chosen. Assuming a Keplerian orbit of the star S0-2 with a semi-major axis of 0.005 pc, Ghez, Salim, Weinberg *et al.* [16]) found an enclosed, central mass of $4.1\times10^6 m_{\odot}$ for Sgr A*. In addition, they deduced an upper-bound on the extended mass of about $0.35\times10^6 m_{\odot}$ within 0.01 pc. Identifying the black hole mass $4.1\times10^6 m_{\odot}$ with $m_s^{\parallel}$(eff) and taking $2m$ equal to $0.35\times10^6 m_{\odot}$, one finds for the arbitrary value $x = 0.99670$ from (7.4) that $\Delta m^{\parallel} = 2.799\, m = 2.799\times½\times0.35\times10^6 m_{\odot} = 0.5\times10^6 m_{\odot}$. Thus, when the orbital planes of S0-2 and both tori coincide, the black hole mass m_s becomes equal to $m_s = m_s^{\parallel}(\text{eff}) - \Delta m^{\parallel} = 3.6\times10^6 m_{\odot}$. Likewise, for the configuration of system B a value for m_s lower than $4.1\times10^6 m_{\odot}$ can be calculated. By choosing again the value $x = 0.99670$ and by averaging the values of $m_s^{\parallel}$(eff) and $m_s^{\perp}$(eff) obtained by a combination of (7.3) through (7.6), an estimated value of $m_s = 3.8\times10^6 m_{\odot}$ can be found. Summing up, mass nearby to the orbit of S0-2 leads to higher values of $m_s^{\parallel}$(eff) and $m_s^{\perp}$(eff) compared with m_s. Thus, the estimate of $m_s = 3.7\times10^6 m_{\odot}$ for Sgr A* used in our calculations may be a reasonable choice.

8. RADIAL ESCAPE OF CHARGE FROM A BLACK HOLE

In order to investigate the origin of jets, the radial motion of a small charge, say a proton, from a star/black hole will be considered. By using Coulomb's law and classical mechanics, it has been shown in sections (2.1) and (2.2), that an equilibrium is possible between a positive charge Q_s of, e.g., black hole, a negative charge Q_i in an inner torus and a positive charge Q_o in an outer torus around the black hole. For convenience sake, both tori are assumed to lie in the same equatorial plane of the black hole (see equations (2.8), (2.17) and figure 5). The electric field from a black hole system consisting of charges Q_s, Q_i and Q_o acting on a small charge e will be described by the Coulomb force, but at short distances from the centre the electric interaction may be different. In this

section we show, that it is possible that a small mass m with charge e, say a proton, may be at rest slightly outside the radius r_{out} of (1.5) for the black hole with positive charge Q_s.

For a small charge moving in a radial direction the relations $d\vartheta = d\varphi = 0$ apply. The Kerr-Newman metric of (1.2) then reduces to

$$ds^2 = \frac{\Delta - a^2 \sin^2\vartheta}{r^2 + a^2 \cos^2\vartheta} c^2 dt^2 - \frac{r^2 + a^2 \cos^2\vartheta}{\Delta} dr^2, \tag{8.1}$$

where Δ is again given by (1.3b). The equations of motion are given by (see, e.g., [21])

$$\frac{d^2 x^\mu}{ds^2} + \Gamma^\mu_{\alpha\beta} \frac{dx^\alpha}{ds} \frac{dx^\beta}{ds} = \frac{e}{mc^2} F^\mu{}_\nu \frac{dx^\nu}{ds}, \tag{8.2}$$

where all parameters have their usual meaning. For radial motion the relevant non-vanishing Christoffel components are

$$\begin{aligned} \Gamma^r_{rr} &= r_g \left\{ \frac{a^2 \cos^2\vartheta - r^2 + \left(a^2/r_g\right) r \sin^2\vartheta + Q_s'^2 r_g r}{\Delta\left(r^2 + a^2 \cos^2\vartheta\right)} \right\}, \\ \Gamma^r_{tt} &= -r_g \Delta \left\{ \frac{a^2 \cos^2\vartheta - r^2 + \left(a^2/r_g\right) r \sin^2\vartheta + Q_s'^2 r_g r}{\left(r^2 + a^2 \cos^2\vartheta\right)^3} \right\}. \end{aligned} \tag{8.3}$$

In addition, the only relevant non-vanishing component of the electromagnetic field tensor is given by

$$F^r{}_t = \frac{-G^{1/2} m_s Q_s' \left(a^2 \cos^2\vartheta - r^2\right) \Delta}{\left(r^2 + a^2 \cos^2\vartheta\right)^3}. \tag{8.4}$$

Assuming that the radial velocity dr/dt equals to zero value, combination of (8.1)–(8.4) yields the following relation

$$\begin{aligned} &\left(r^2 - 2 r_g r + a^2 \cos^2\vartheta + Q_s'^2 r_g{}^2\right)^{1/2} Q_s' \left(r^2 - a^2 \cos^2\vartheta\right) = \\ &\frac{G^{1/2} m}{e} \left\{ r^2 - a^2 \cos^2\vartheta - \left(a^2/r_g\right) r \sin^2\vartheta - Q_s'^2 r_g r \right\} \left(a^2 \cos^2\vartheta + r^2\right)^{1/2}. \end{aligned} \tag{8.5}$$

Note that the quantity $G^{1/2} m/e$ is a very small dimensionless number (for a proton $G^{1/2} m/e = + 8.996 \times 10^{-19}$).

For the limiting case of the Reissner-Nordstrøm space-time (see, e.g., ref. [18]) the specific angular momentum a is zero, so that the condition (8.5) simplifies to

$$\left(r^2 - 2 r_g r + Q_s'^2 r_g{}^2\right)^{1/2} = \frac{G^{1/2} m}{e Q_s'} r \left\{1 - Q_s'^2 \left(r_g/r\right)\right\}. \tag{8.6}$$

Note that relation (8.6) does not depend on ϑ. The solution with the highest value for r from (8.6) can be written in terms of $r = r_g(1 + \delta')$, where δ' is approximately given by

$$\delta' = \left(1-Q_s'^2\right)^{1/2} + \varepsilon^2\left(1-Q_s'^2\right)^{1/2}\left\{1-\tfrac{1}{2}Q_s'^2+\left(1-Q_s'^2\right)^{1/2}\right\}. \tag{8.7}$$

Here ε is defined by $\varepsilon \equiv G^{1/2}m/(eQ_s')$. This value can be compared with the corresponding radii $r_+ = r_{out} = r_g(1+\delta)$ (see (1.4) and (1.5) for $a = 0$), where

$$\delta = \left(1-Q_s'^2\right)^{1/2}. \tag{8.8}$$

As an example, for a value like $Q_s' = 0.3009$ for Sgr A* (see section 6.3) δ obtains the value $\delta = 0.954$, so that δ' is then slightly more positive than δ (see (8.7)). Since the term containing ε^2 in (8.7) is small, δ' can be approximated by δ. As a result, the equatorial radius r_{out} reduces to $r_{out} = 1.954\,r_g$. Note that the magnitude of Q_s' in relations (8.7) and (8.8) is only limited by $Q_s'^2 \leq 1$. Therefore, apart from this upper limit, no maximum follows for charge added to charge Q_s' in (8.7) at radius of $r = r_g(1+\delta')$. The values of δ' and δ, and the corresponding radii, however, do depend on the value of Q_s'.

Since the quantity $G^{1/2}m/e$ in (8.5) is so extremely small, the right hand side of (8.5) can generally be approximated by zero value. Assuming that $Q_s' > 0$ and $a^2 - r^2\cos^2\vartheta \neq 0$, the two solutions r_{in} and r_{out} of (1.5) for r result. For this reason, these radii may be interpreted as two possible equilibrium locations for a small positive charge near the centre of the black hole. For a small value of $G^{1/2}m/e$, the condition of a radial velocity $dr/dt = 0$ is thus equivalent to the condition $g_{tt} = 0$, leading to the relations of (1.5).

For a proton located on the rotation axis $\mathbf{s} = \boldsymbol{\Omega}_s/\Omega_s$ of the black hole (i.e., $\vartheta = 0$), two values for r exist, where the proton may be at rest. From (1.4) and (1.5) then follow the radii $r_- = r_{in} = r_g - (r_g^{\,2} - a^2 - Q_s'^2 r_g^{\,2})^{1/2}$ and $r_+ = r_{out} = r_g + (r_g^{\,2} - a^2 - Q_s'^2 r_g^{\,2})^{1/2}$.

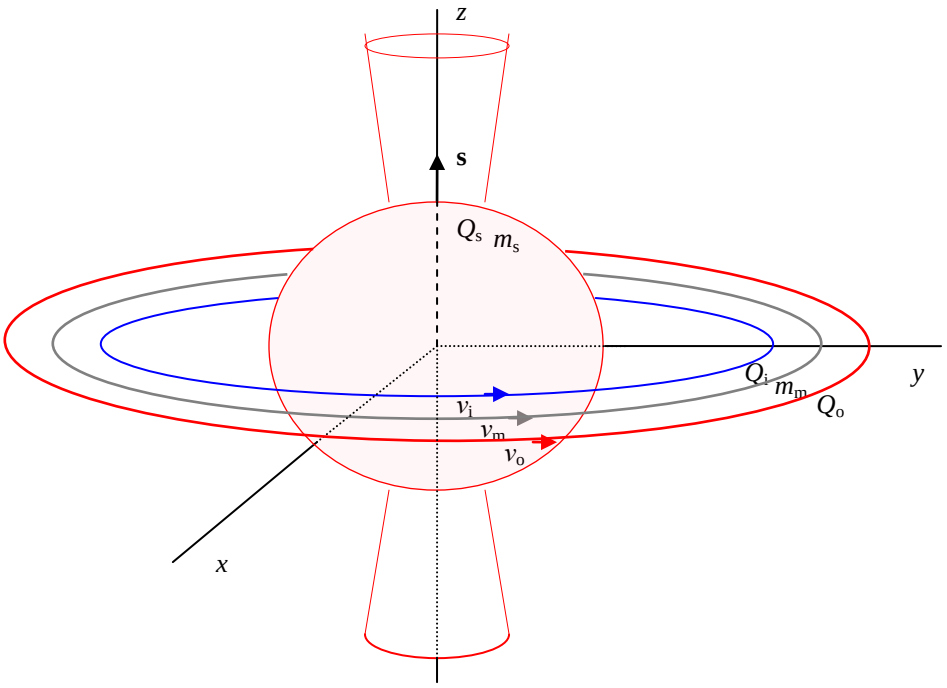

Figure 5. Scheme of jet model for a black hole like Sgr A* with a shell of positive charge Q_s (red) and mass m_s. The unit vector along the rotation axis of the star is $\mathbf{s} \equiv \boldsymbol{\Omega}_s/\Omega_s$. The unit vectors perpendicular to the circular tori with negative charge Q_i (blue), mass m_m (grey) and charge Q_o (red) all coincide with unit vector $\mathbf{s}$. The frequencies of the various tori with charge Q_i, mass m_m and charge Q_o are denoted by v_i, v_m and v_o, respectively. It has been assumed that $r_i = r_{ISCO}$.

Another limiting case occurs at large distance from the centre of the black hole ($r >> r_g$). Then, combination of (8.1)–(8.4) yields the following non-relativistic result for the radial force

$$m\frac{d^2r}{dt^2} = -\frac{mGm_s}{r^2} + \frac{eQ_s}{r^2} = \frac{eQ_s}{r^2}(1-\varepsilon). \tag{8.9}$$

From this relation it follows that, e.g., a proton with mass m and charge e in presence of mass m and a positive charge Q_s is attracted by the Newtonian force and repelled by the Coulomb force. For example, for $Q_s' = 0.3009$ the quantity ε is much smaller than unity value, so that the Coulomb force strongly dominates. It is noticed that for a system, consisting of a star with charge Q_s and two equatorial, charged tori with charges and Q_i and Q_o, a detailed expression for the electric field at the north pole of the star with radius r_s has previously been calculated [10]. Both expression (8.9) and the result of ref. [10], demonstrate the importance of Coulomb repulsion along the rotation axis of a black hole. As an illustration of our analysis figure 5 has been added.

Summing up, for a black hole with a positive relative charge Q_s' a proton with mass m and charge e is strongly repelled by the standard Coulomb force. For a non-rotating black hole ($a = 0$) and a value of $Q_s' > 0$, however, the proton may be at rest at distance r slightly larger than $r_{out} = r_g + r_g(1-Q_s'^2)^{½}$ from the centre of the black hole (compare (8.7) and (8.8)). For a fast rotating black hole, the proton may be at rest on the rotation axis of the black hole, at a distance r slightly larger than $r_{out} = r_g + (r_g^2 - a^2 - Q_s'^2 r_g^2)^{½}$ from the centre. Such a proton may combine with the large positive charge Q_s.

More generally, the presented investigation of the radial motion of a small charge e near a black hole, pulsar or other star with charge Q_s may give some key ingredients for the explanation of observed jets. At larger distances from the star a proton located on the rotation axis may be accelerated up to relativistic velocities by the Coulomb repulsion, for example, due to charge Q_s, but at short distance from the centre the charge Q_s may be bound on a shell with radius given by r_{out} of (1.5). When external charges Q_i and Q_o are present in two equatorial circular tori, an additional charge equilibrium may exist in the equatorial plane between the charges Q_s, Q_i and Q_o. Accretion may distort the latter charge equilibrium and may induce a charge burst mainly along the rotation axis of the star. See figure 5 as an illustration.

9. DISCUSSION OF THE THREE TORI MODEL

In this work three high frequency quasi-periodic oscillations (QPOs) of the black holes Sgr A* and XTE J1550–564 are attributed to three different circular tori: an inner torus with charge Q_i, a torus with electrically neutral mass m_m and an outer torus with charge Q_o. The corresponding QPO frequencies ν_i, ν_m and ν_o of the massive black hole Sgr A* and the stellar black hole XTE J1550–564 follow the sequence $\nu_i > \nu_m > \nu_o$, whereas the values of the corresponding radii follow the sequence $r_i < r_m < r_o$. The frequencies ν_i, ν_m and ν_o, and the radii r_i, r_m and r_o for these black holes are presented in section 6 and are summarized in table 4. All radii, however, are now expressed in units of the gravitational radius r_g of the considered black hole.

Generally spoken, the nature of the observed frequencies is "quasi-periodic". Thus, different measurements often yield slightly different values for the same QPO frequency, whereas one ore more QPO frequencies may be weak or even absent. For XTE J1550–564 this problem has previously been discussed (see, e.g., [10]). For Sgr A* different values for the QPO periods/frequencies are reported by Miyoshi *et al.* [2] and Aschenbach *et al.* [3, 4]. In the future, more reliable QPO frequencies than summarized in table 3 may be observed for Sgr A*.

In addition, the identification of the various QPO frequencies is a major issue. As

an illustration, we compare the identification of the Kepler-like frequency ν_m of (6.2) for XTE J1550–564 in some models. Stella and Vietra (see, e.g. ref. [5]), for example, attributed the highest observed QPO frequency ν_u to ν_m in their relativistic precession model. Schnittman and Bertschinger [8], however, motivated by the resonance model of Kluźniak and Abramowicz [6,7], analysed five observed QPO frequencies of XTE J1550–564 and attributed the second highest QPO frequency 276 Hz to ν_m (corresponding to 268 Hz in our table 4). A resonance $\nu_r:\nu_m = 1:3$ was adopted in their analysis. Török [9], also following the model of refs. [6, 7], attributed the high QPO frequencies 276 Hz to ν_u and 184 Hz to ν_l, respectively, (corresponding to 268 Hz and 188 Hz in our table 4) for XTE J1550–564. Considering the resonance $\nu_r:\nu_m = 1:3$, in combination $\nu_u = \nu_m$ and $\nu_l = \nu_m - \nu_r$, yields the ratio $\nu_u/\nu_l = 2/3$ (in agreement with observations) and a value $a = +0.43r_g$ for a mass $m_s = 9.61\ m_\odot$. Additional resonances between ν_r and ν_m or ν_v were discussed by Török [9], e.g., $\nu_r:\nu_m = 1:2$, in combination $\nu_u = \nu_m + \nu_r = 276$ Hz and $\nu_l = \nu_m = 184$ Hz, resulting into a theoretical ratio $\nu_u/\nu_l = 3/2$ and a value $a = +0.29r_g$. Finally, in our three tori model for XTE J1550–564 we identify ν_m with the second highest frequency of 188 Hz. From our three tori model, however, no value for a follows.

For the supermassive black hole Sgr A* the identification of the Kepler-like frequency ν_m is even more difficult. For example, Aschenbach *et al.* [3] gave an interpretation of four QPO frequencies in terms of the frequencies ν_{LT} (our equation (3.11)), ν_m, ν_v and ν_r. In their so-called low mass solution they attributed the extracted QPO frequency 4.562 mHz to ν_m, but later on Aschenbach [4] concluded, that more recent measurements gave no confirmation for QPO frequencies higher than about 1.5 mHz. Török [9] (compare with our table 3) only identified two QPO frequencies for Sgr A*: 1.445 mHz and 0.886 mHz with ν_u and ν_l, respectively. When a resonance $\nu_r:\nu_m = 1:3$ is adopted, the combination $\nu_u = \nu_m$ and $\nu_l = \nu_m - \nu_r = 0.886$ mHz, then results into the ratio $\nu_u/\nu_l = 3/2$ and a value 1.329 mHz for ν_u (instead of the observed value 1.445 mHz). In addition, a value $a = +0.86r_g$ then follows from the chosen mass $m_s = 3.7\times10^6\ m_\odot$. Alternatively, the choice $\nu_r:\nu_m = 1:2$, in combination with $\nu_u = \nu_m + \nu_r$ and $\nu_l = \nu_m = 0.886$ mHz, leads again to the ratio $\nu_u/\nu_l = 3/2$ and $\nu_u = 1.329$ mHz, whereas a changes into $a = +0.84r_g$. For both considered resonances the theoretical ratio $\nu_u/\nu_l = 3/2$ differs from the observed ratio $\nu_u/\nu_l = 1.63$. Finally, we have chosen $\nu_m = 0.992$ mHz from the reported data of Miyoshi *et al.* [2]. In conclusion, no QPO frequency for Sgr A* (or any other star!) has definitively been identified with the Kepler-like frequency ν_m.

Table 4. Summary of frequencies ν_i, ν_m and ν_o and radii r_i, r_K, r_m, r_o and r_{ISCO} (see tables 2 and 3) for the stellar black hole XTE J1550–564 and the massive black hole Sgr A*.

Black hole	ν_i	ν_m	ν_o		r_i (r_g)	r_m/r_K (r_g)	r_o (r_g)	r_{ISCO}[g] (r_g)
	(Hz)	(Hz)	(Hz)			r_K		
				r_K[c]	5.40	6.84	14.19	
XTE J1550–564[a]	268	188	62.9	$a = 0$[d]	6.05	6.84	8.28	5.98
						r_m		
				$a = r_g$[e]	5.82	6.58	7.97	$F > 0$
	(mHz)	(mHz)	(mHz)			r_K		
				r_K[c]	3.58	4.26	5.13	
Sgr A*[b]	1.29	0.992	0.751	$a = 0$[f]	3.88	4.26	4.56	5.85
						r_m		r_i
				$a = 0.584r_g$[f]	3.71	4.07	4.35	3.71
				$a = r_g$[f]	3.58	3.93	4.21	$F > 0$

[a] Used mass $m_s = 9.61\ m_\odot$. [b] Used mass $m_s = 3.7\times10^6 m_\odot$. [c] Kepler radii are calculated from (6.3). [d] Radius r_K calculated from (6.3). See ref. [10] for the calculation of r_i and r_o. [e] Calculated from (6.2), using $S = cm_sa$. See section 6.2 for the calculation of r_i and r_o. [f] See section 6.3. [g] Values of r_{ISCO} are calculated from (1.6). A stable circular orbit occurs for r_i, when $r_i \geq r_{ISCO}$, or when $F \geq 0$ in (1.6). For $a = 0.584r_g$ the assumption $r_i = r_{ISCO}$ has been made.

Table 4 shows that calculated radii r_i for XTE J1550–564 slightly differ from the value of the radius of the innermost stable circular orbit radius in Schwarzschild space-time, $r_{ISCO} = 6Gm_s/c^2$. In Reissner-Nordstrøm space-time, a value of $r_{ISCO} = 5.98\,r_g$ is obtained from (1.6) for $a = 0$ and $Q_s' = 0.1009$, compatible with the value $r_i = 8.585\times10^6$cm $= 6.05\,r_g$ deduced in ref. [10]. For $a = r_g$ and $Q_s' = 0.0971$ in Kerr-Newman space-time, a stable circular orbit of radius $r_i = 8.262\times10^6$cm $= 5.82\,r_g$ follows from (1.6) ($F > 0$). For details see table 2. No preference value for a can be extracted for XTE J1550–564 from our three tori model.

For Sgr A* table 4 shows the calculated Kepler radius $r_K = 2.330\times10^{12}$cm $= 4.263\,r_g$ (see section 6.3) and radius $r_i = 2.123\times10^{12}$cm $= 3.885\,r_g$ from relation $r_i = x_i\,r_K$. Both radii are incompatible with the innermost stable circular orbit $r_{ISCO} = 5.85\,r_g$ in Reissner-Nordstrøm space-time, calculated from (1.6) for $F = 0$, $a = 0$ and $Q_s' = 0.3150$. Alternatively, choosing value $a = r_g$, radius r_i can be calculated from $r_m = 2.150\times10^{12}$cm $= 3.933\,r_g$, resulting into $r_i = x_i\,r_m = 0.91137\times2.150\times10^{12}$cm $= 1.959\times10^{12}$cm $= 3.585\,r_g$. From (1.6) follows that the circular orbit for $r_i = 3.585\,r_g$, $a = r_g$ and $Q_s' = 0.2907$ is stable ($F > 0$). Assuming $r_i = r_{ISCO}$, it appears possible to find a unique value for the ratio a/r_g by combination of the relations (1.6) for $F = 0$, (6.2) and $r_i = x_i\,r_m$. Application of the iteration process yields: $a/r_g = +\,0.584$ for $r_m = 4.072\,r_g$, $r_i = 3.711\,r_g$ and $Q_s' = 0.3009$. The latter value of r_i can be compared with the equatorial radius r_{out} from (1.5). Substitution of $a = +\,0.584\,r_g$, $\vartheta = 90^o$ and $Q_s' = 0.3009$ into (1.5) yields $r_{out} = 1.954\,r_g$. In view of uncertainties in the extracted QPO frequencies and their assignments, however, the magnitude of a for Sgr A* remains uncertain.

In table 5 the assigned low frequency QPOs ν_{mo}, ν_{io}, ν_{mi} and ν_{oi} from (6.4)–(6.7) for the black holes from tables 2 and 3 have been summarized. In addition, the relative charges Q_i', Q_o' and Q_s' (Q_i' is defined by $Q_i' \equiv (G^{½}m_s)^{-1}Q_i$ and so on) have been added. It appears that the average value of the relative charges Q_s' of both black holes amount to about 0.2, whereas an average value of Q_s' about 0.33 has previously been calculated for four pulsars [10].

Table 5. Summary of frequencies ν_{mo}, ν_{io}, ν_{mi} and ν_{oi}, relative charges Q_s', Q_i' and Q_o' from tables 2 and 3 for two black holes.

Black hole	ν_{mo}	ν_{io}	ν_{mi}	ν_{oi}	a	Q_i'	Q_o'	Q_s'
	(Hz)	(Hz)	(Hz)	(Hz)				
XTE J1550–564[a]	8.75	5.04	4.090	0.73	0 r_g	–0.070 –0.068	+0.447 +0.430	+0.101 +0.097
	(mHz)	(mHz)	(mHz)	(mHz)				
Sgr A*[b]	0.531	0.296	0.130	0.0622	0 0.584r_g r_g	–0.159 –0.152 –0.146	+0.492 +0.470 +0.454	+0.315 +0.301 +0.291

[a] Used mass $m_s = 9.61\,m_\odot$. [b] Used mass $m_s = 3.7\times10^6\,m_\odot$.

For both black holes seven observed QPO frequencies in tables 4 and 5 have been identified with the seven predicted QPO frequencies of our model. The resonance model of Kluźniak and Abramowicz [6,7], only accounts for two QPO frequencies. In their analysis of the QPO frequencies of XTE J1550–564 by Schnittman and Bertschinger [8] the latter model has, however, been extended up to five QPO frequencies, the Lense-Thirring precession $\overline{\nu_{LT}}$ (our equation (3.11)) included. The relativistic precession model given by Stella, Vietri (see, e.g., [5]) only accounts for three basic QPO frequencies, when the Lense-Thirring precession frequency $\overline{\nu_{LT}}$ is included. Furthermore, Aschenbach *et al.* [3] gave an interpretation of four (or five) QPO frequencies for Sgr A* in terms of the frequencies $\overline{\nu_{LT}}$, ν_m, ν_v and ν_r.

Since the rotation frequency v_s is unknown and the stellar radius r_s has not been defined for black holes, the Lense-Thirring precession frequency v_{LT} of a torus cannot be calculated from (3.10b). Combination of (3.10a), the extreme value of the angular momentum S from (3.3) and radius $R = r_i$, however, yields a value for the Lense-Thirring precession $v_{LT}(m_i)$ of the inner torus with mass m_i. Since the orbit of this torus is close to the black hole, the magnetic dipole approximation for the black hole may no longer be valid and the value of $v_{LT}(m_i)$ may become smaller (see ref. [22] and comment to (3.10)). Moreover, in our approach the gravitomagnetic field has been identified with a magnetic field. Calculated values for the Lense-Thirring frequencies $v_{LT}(m_i)$ for both black holes are given in sections 6.2 and 6.3. To my knowledge, however, no unambiguous identification of any Lense-Thirring frequency in any stellar system has yet been made.

10. CONCLUSIONS

A model with three circular tori has recently been proposed [10] in order to explain the quasi-periodic oscillations (QPOs) of pulsars, black holes and white dwarfs. Apart from the Lense-Thirring precession frequency v_{LT} (see equations (3.10) and (3.11), seven QPO frequencies are predicted in our model: three high frequency QPOs (v_i, v_m and v_o) and four low frequency QPOs (v_{mo}, v_{io}, v_{mi} and v_{oi}). Details are given in sections 2 and 4, and figure 3 is added as an illustration.

Reported QPO frequencies of the stellar black hole XTE J1550–564 and the supermassive black hole Sgr A* are compared with the seven QPO frequencies predicted by the new model. A good fit for both black holes could be found between observed and predicted frequencies, but two parameters had to be estimated. The results of most calculations are summarized in tables 4 and 5 and are compared with other models [4–9] in section 9. Moreover, for both black holes an estimate of the Lense-Thirring precession frequency ν_{LT} for an approximately equatorial orbit is given in section 6.

Summing up, the three tori model seems to be in agreement with more observations than previously proposed models. In view of the intermittent character of QPOs and uncertainty in their assignment, however, definite conclusions about the proposed model cannot yet be drawn.

In our analysis a precise value of the mass of Sgr A* is desirable. We shortly discussed available mass values [15–17] in section 7. The mass m_s of Sgr A*, for example, has been deduced from the orbit of star S0-2 around the black hole [16], so that enclosed mass within the orbit of S0-2 may contribute. In section 7 we deduce new expressions for the effective mass m_s (eff) of a black hole acting on a companion star of mass m_c ($m_c << m_s$), moving in a circular orbit around the black hole. It appears that the calculated effective mass m_s(eff) becomes larger than m_s by the presence of a massive torus in a circular orbit around the black hole. In addition, m_s(eff) becomes *anisoptropic*: its value depends on the orientation of the orbital plane of the torus. Results are qualitatively compared with reported mass values for Sgr A*. Moreover, the analysis reveals another peculiar effect, when the orbital planes of torus and companion star are perpendicular to each other. An initially circular orbit of the companion star around the black hole may become approximately elliptical with, e.g., Sgr A* located *in the centre* of the ellipse (*not in a focal point!*).

Finally, the origin of jets is considered in section 8. Starting from the Kerr-Newman metric, radial motion of a small mass m with charge e, say a proton, near a black hole, pulsar or other star is investigated. It appears that a proton may be bound on a shell, slightly outside the outer radius r_{out} of a black hole with (positive) charge Q_s. At larger distances from the centre of the black hole, however, protons can be accelerated up to relativistic velocities by the dominating Coulomb force. When external charges Q_i and Q_o are present in two circular the tori in the equatorial plane, an additional charge equilibrium may exist between the charges Q_s, Q_i and Q_o. Accretion may distort the latter charge equilibrium and may induce a charge burst mainly along the rotation axis of the

star. Figure 5 is given as an illustration.

ACKNOWLEDGEMENT

The technical help of my son Pieter in publishing this paper is gratefully acknowledged.

REFERENCES

[1] van der Klis, M., "Rapid X-ray variability." In: *Compact stellar X-ray sources* (Eds. Lewin, W. and van der Klis, M.), Cambridge University Press, Cambridge, Chapter 2 (2006); arXiv:astro-ph/0410551v1, 22 Oct 2004.

[2] Miyoshi, M., Zhi-Qiang Shen, Oyama, T., Takahashi, R. and Kato, Y., "Oscillation phenomena in the disk around the massive black hole Sagittarius A*." arXiv:0906.5511v1 [astro-ph.HE], 30 Jun 2009 and references therein.

[3] Aschenbach, B., Grosso, N., Porquet, D. and Predehl, P. "X-ray flares reveal mass and angular momentum of the Galactic Center black hole." *Astron. Astrophys.* **417**, 71-78 (2004).

[4] Aschenbach, B. "Measurement of mass and spin of black holes with QPOs." *Chin. J. Astron. Astrophys. (Supplement)* **8**, 291-296 (2008).

[5] Stella, L., Vietri, M. and Morsink, S. M., "Correlations in the quasi-periodic oscillation frequencies of low-mass X-ray binaries and the relativistic precession model." *Ap. J.* **524**, L63-L66 (1999).

[6] Kluźniak, W. and Abramowicz, M. A., "The physics of kHz QPOs --- strong gravity 's coupled anharmonic oscillators." *arXiv:astro-ph*/0105057v1, 3 May 2001 (submitted to *Phys. Rev. Letters*).

[7] Abramowicz, M. A. and Kluźniak, W., "A precise determination of black hole spin in GRO J1655-40." *Astron. Astrophys.* **374**, L19-20 (2001).

[8] Schnittman, J. D. and Bertschinger, E., "A model for high frequency quasi-periodic oscillations from accreting black holes." *Ap. J.* **606**, 1098-1111 (2004).

[9] Török, G., "QPOs in microquasars and Sgr A*: measuring the black hole spin." *Astron. Nachr.* **326**, 856-860 (2005).

[10] Biemond, J., "Quasi-periodic oscillations, charge and the gravitomagnetic theory." arXiv:0706.0313v2 [physics.gen-ph], 20 Mar 2009.

[11] Biemond, J., *Gravi-magnetism*, 1st ed. (1984). Postal address: Sansovinostraat 28, 5624 JX Eindhoven, The Netherlands. E-mail: gravi@gewis.nl Website: http://www.gewis.nl/~pieterb/gravi/

[12] Biemond, J., *Gravito-magnetism*, 2nd ed. (1999). See also ref. [11].

[13] Biemond, J., "The origin of the magnetic field of pulsars and the gravitomagnetic theory." In: *Trends in pulsar research* (Ed. Lowry, J. A.), Nova Science Publishers, New York, Chapter 2 (2007) (updated and revised version of arXiv:astro-ph/0401468v1, 22 Jan 2004).

[14] Biemond, J., "Which gravitomagnetic precession rate will be measured by Gravity Probe B?", arXiv:physics/0411129v1 [physics.gen-ph], 13 Nov 2004.

[15] Ghez, A. M., Salim, S., Hornstein, S. D., Tanner, A., Lu, J. R., Morris, M., Becklin, E. E. and Duchêne, G., "Stellar orbits around the Galactic Center black hole." *Ap. J.* **620**, 744-757 (2005).

[16] Ghez, A. M., Salim, S., Weinberg, N. N., Lu, J. R., Do, T., Dunn, J. K., Matthews, K., Morris, M., Yelda, S., Becklin, E. E., Kremenek, T. Milosavljevic, M. and Naiman, J., "Measuring distance and properties of the Milky Way's central supermassive black hole with stellar orbits." *Ap. J.* **689**, 1044-1062 (2008).

[17] Schödel, R., Merritt, D. and Eckart, A., "The nuclear star cluster of the Milky Way: Proper motions and mass." *Astron. Astrophys.* **502**, 91-111 (2009).

[18] Misner, C. W., Thorne, K. S. and Wheeler, J. A., *Gravitation*, W. H. Freeman and Company, San Francisco, Chapter 33 (1973).

[19] Dadhich N. and Kale, P. P., "Equatorial circular geodesics in the Kerr-Newman geometry." *J. Math. Phys.* **18**, 1727-1728 (1977).

[20] Gradshteyn, I. S. and Ryzhik, I. M., *Tables of integrals, series, and products*, 5th ed., (Ed. Jeffrey, A.), Academic Press, Boston, (1994).

[21] Aliev, A. N. and Galtsov, D. V., "Radiation from relativistic particles in nongeodesic motion in a strong gravitational field." *Gen. Rel. Grav.* **13**, 899-912 (1981).

[22] Biemond, J., "The gravitomagnetic field of a sphere, Gravity Probe B and the LAGEOS satellites", arXiv:0802.3346v1 [physics.gen-ph], 22 Feb 2008.

[23] Ballantyne, D. R., Melia, F., Liu, S. and Crocker, R. M., "A possible link between the Galactic Center HESS source and Sagittarius A*." *Ap. J.* **657**, L13-L16 (2007).